Computational analysis of magnetohydrodynamics boundary layer flow of nanofluid over a stretching sheet in the presence of heat generation or absorption and chemical reaction

by

MOLAUDZI VHUTSHILO

11600837

Research for the Master of Science in the Department of Mathematics and Applied Mathematics

School of Mathematical and Natural Sciences

University of Venda

Thohoyandou, Limpopo

South Africa

Supervisor: Prof S. Shateyi

Co-supervisor: Dr K. Muzhinji

2021

Abstract

In this study, we present the effect of two-dimensional magnetohydrodynamics of a nanofluid over a stretching sheet in the presence of chemical reaction, as well as heat generation or absorption. The partial differential equations are reduced to coupled nonlinear ordinary differential equations using similarity transformations, which are then solved numerically using spectral local linearization and spectral relaxation methods. The effects of different parameters, Lewis number, Eckert number, stretching, chemical reaction, local Reynolds number, Prandtl number, constant, heat source, Brownian motion, and Thermophoresis are analysed and compared. The numerical results for velocity, temperature, skin friction coefficient, concentration, Sherwood number, and Nusselt number are presented in tabular form and visualized graphically. The findings of the spectral local linearization and spectral relaxation methods are very similar to the bvp4c method's results. When compared to the spectral relaxation method, the results from the spectral local linearization method were more effective. We found that the velocity profile are increased with increasing values of the Grashof number (Gr). Since Grashof number (Gr) is ratio of buoyancy to viscous forces in the boundary layer it causes an increase in the buoyancy forces relative to the viscous forces which influence the velocity in the boundary layer region. An increase in the heat source/sink parameter (S) results in the increase in velocity and temperature, but a decrease in concentration. The concentration diffusion species were reduced due to the heat source/sink parameter (S). The results also show that heat generation increases the momentum and thermal boundary layer thickness while decreasing the nanofluid concentration boundary layer thickness.

Keywords: boundary layer flow; heat transfer; mass transfer; nanofluid; magnetohydrodynamics; heat generation/absorption; chemical reaction; thermophoresis; spectral local linearisation method; spectral relaxation method.

Nomenclature

u	velocity component in the x-direction
v	velocity component in the y-direction
x	direction coordinate
y	direction coordinate
B_0	induced magnetic field strength
k	thermal conducivity
T	temperature of nanofluid
$(\rho c)_f$	heat capacitance of the base fluid
$(\rho c)_p$	heat capacitance of the nanoparticles
D_B	Brownian diffusion coefficient
D_T	thermophoresis diffusion coefficient
M	magnetic parameter
Pr	Prandtl number
Le	Lewis number
C	concentration of nanofluid
Nb	Brownian motion parameter
Nt	thermophoresis parameter
C_w	specific heat capacity of the nanoparticle
Re_x	local Reynolds number
q_r	radiative heat flux
C_{fx}	skin-friction coefficient
C_w	temperature along the stretching sheet
T_w	concentration along the stretching sheet
T_∞	ambient temperature
C_∞	ambient concentration
m	constant parameter
R	radiation parameter
Ec	Eckert number
S	heat generation/sink parameter
l	characteristics length
λ	stretching constant
k^*	mean absorption coefficient
Q	heat generation/absorption coefficient
U_w	stretching sheet wall velocity
β_t	thermal expansion coeffient
β_c	concentration expansion coeffient
g	gravitational acceleration
K_o	chemical reaction parameter

Greek symbols

σ	Stefan-Boltzmann
α	thermal diffusivity
ρ	density of the nanofluid
η	transformed variable
γ	chemical reaction parameter
ψ	stream function
ϕ	dimensionless species concentration
θ	dimensionless temperature

Abbrevations

SLLM - Spectral Local Linearization Method
SRM - Spectral Relaxation Method
MHD - Magnetohydrodynamics
PDE - Partial Differential Equation
ODE - Ordinary Differential Equation
SIM - Simple Iteration Method

Declaration

I, **Vhutshilo Molaudzi** [**student number: 11600837**], proclaim that the work contained in this project is my work and this has not been submitted to any other university or institution for the award of any degree. The work done by others has been acknowledged and referenced accordingly.

Signature (Student): V. Molaudzi Date: 04/10/2021

Acknowledgment

I would like to acknowledge the following for their help and support regarding this research;

- Prof. S. Shateyi, my supervisor for his warmth, guidance, encouragement throughout the entire study.
- I would also like to thank my co-supervisor Dr. K. Muzhinji for his support and patience throughout my research.
- Dr. S Moyo, the HOD of Department of Mathematics and Applied Mathematics for his support toward accomplishment of the study.
- Prof. N Potgieter, former DEAN of School of Mathematical and Natural Sciences for allowing me to do my masters at the school.
- Mrs. N. Mukwevho, Mr. N. Ndou, Mr. A. Manthada, Dr. D. Mathebula, Ms. AD. Maphiri and Mrs. RM. Mukhodobwane, my colleagues who encouraged me continuously.
- I would like to say to my family and relatives bless you all for supporting me throughout the hardest time of my research, especially my mother Selina Molaudzi my hero in my struggle.

Publication

Part of the work in this thesis has been submitted for publication and is published.

Molaudzi V, Shateyi S and Muzhinji K, Computational analysis of magnetohydrodynamics boundary layer flow of nanofluid over a stretching sheet in the presence of heat generation or absorption and chemical reaction. *JP Journal of Heat and Mass Transfer*, Volume 24, pp 157 - 189, 2021.

Contents

List of Tables

List of Figures

Chapter 1

Introduction

This chapter introduces the problem statement, research question, purpose of the study, aim and objectives of the study. The chapter also discusses the background to the study and definition of key terms.

1.1 Background

In this study, we focus on the heat generation/absorption and chemical reaction effects with viscous dissipation on MHD boundary layer flow. The study of boundary layer flow began in 1904 by German engineer called Ludwing Prandtl, who wrote perhaps the most important article on fluid mechanics. Prandtl presented a paper on the motion of fluid flow with small viscosity (water and air flow) at the Third International Congress of Mathematics, Anderson [9]. The boundary layer flow theory have been proven to be the single most important tool in modern flow analysis Ibrahim and Tulu [19]. The analysis of MHD flow and heat transfer has been given much attention because of the effect of magnetic field on the boundary layer flow control and on the performance systems using electrically conducting fluids.

The study of heat generation/absorption and chemical reaction in moving fluids is of practical importance to many processes in several branches of science and technology. The engineering application involves chemical distillation process, formation and dispersion of fog, channel type solar energy collectors and thermo-protection systems, Kuppala *et al.*[27]. Chemical reaction can be classified as heterogeneous or homogeneous. This depends on whether they occur as a single phase volume reaction or chemical reaction is of first order, if the rate of reaction is directly proportional to the species concentration. Sarojamma *et al.* [39] investigated the influence of Hall currents on cross diffusive convection in a MHD boundary layer flow on stretching sheet in porous medium with heat generation. Shateyi and Marewo [42] also studied numerical analysis of unsteady MHD flow near a stagnation point of two dimensional porous bodies with heat and mass transfer thermal radiation and chemical reaction. The effect of chemical reaction and heat generation/absorption on unsteady mixed

convection MHD flow over a vertical cone with non-uniform slot mass transfer was analyzed by Ravindran *et al.* [38]. Shateyi and Motsa [46] studied unsteady magnetohydrodynamics convective heat and mass transfer past an infinite vertical plate in a porous medium with thermal radiation heat generation/absorption and chemical reaction.

1.2 Problem statement

This project is briefly described above, the work jointly with effects of chemical reaction, heat generation or absorption, buoyancy force thermal expansion, buoyancy force concentration expansion. The study focus on boundary layer flow and heat transfer characteristics on the MHD of nanofluid over stretching sheet.

1.3 Research question

How effective are the proposed numerical methods in the numerical solution process of the steady MHD boundary layer flow and heat transfer characteristics in the presence of chemical reaction effects of nanofluid over stretching sheet?

1.4 Purpose of the study

The purpose of this project is to numerically analyze the effects heat generation/absorption, chemical reaction, buoyancy force thermal expansion, buoyancy force concentration expansion on boundary layer flow and heat transfer characteristics on the MHD of nanofluid over stretching sheet in the presence of thermal radiation and viscous dissipation.

1.5 Aim and objectives

Aim

To analyse the steady state MHD boundary layer flow and heat transfer that characterise free convection flow in the presence of heat generation/absorption, thermal radiation viscous dissipation, chemical reaction of nanofluid over stretching sheet.

The objectives of the study are to:

(i) Formulate a mathematical model of steady MHD flow and heat transfer characteristics in the presence of heat generation/absorption and chemical reaction of a nanofluid over a stretching sheet.

(ii) Transform the partial differential equations (PDEs) of the governing equations into ordinary differential equations (ODEs) by using similarity variables.

(iii) Determine the numerical solution of ODEs using spectral relaxation method and spectral local linearization method.

(iv) Investigate the effect of permeable sheet and other governing parameters on steady MHD boundary layer flow and heat transfer characteristics in the presence of heat generation/absorbption and chemical reaction of a nanofluid over a stretching sheet in order to get an engineering point of view.

1.6 Definition of Keywords

Thermal radiation: is one of three ways for exchanging energy between bodies of different temperatures. The emission of electromagnetic waves from the substance characterizes thermal radiation (variation of its internal energy). It transmits radiation ranging from ultraviolet to far field infrared depending on the temperature of the substance. The entire body functions as a continuous emitter of thermal radiation as well as a continuous receiver of radiation from far-field bodies. Thermal radiation, on the other hand, is linked to the transmitter's, receiver's, and crossed medium's molecular structure, Derobert and Dumoulin [14].

Brownian motion: is a random movement of microscopic molecule suspended in fluids or gases coming about because of the effect of atoms of the fluid surrounding the particles and furthermore called Brownian developments, Parimal [37].

Thermophoresis: is observed in blends of versatile particles where the various particles and where the diverse molecule types show various reactions to the force of a temperature gradient, Brinker [8].

Magnetohydrodynamics (MHD): is defined as the investigation of magnetic properties and practices of electrically directing fluids, at that point model magneto liquids incorporate fluid, plasma, salt water, metals and electrolytes, Alfvé [2].

Steady flow and unsteady flow: a steady flow is where the flow parameters such as velocity, pressure, and density are independent of time, whereas in an unsteady flow, they are dependent on time. Flow in a pipe of variable diameter with a constant pressure head is an example of steady flow (e.g reservoir of tank). Unsteady flow can be described as flow via a pipe of variable diameter under varied pressure caused by changes in the reservoir's water level, the opening or closing of a valve, or the stopping or starting of hydraulic devices connected to the pipe. Landau [29].

Incompressible flow: refers to the fluid flow where the fluid thickness steady for a thickness to stay constant, the control volume needs to stay even through the pressure changes the thickness will be consistent for an incompressible stream with variety of thickness because of pressure changes is irrelevant or infinitesimal. Fluid at steady temperature is incompressible, Anderson [4].

Compressible flow: means a flow that experiences prominent variety in thickness with trending pressure thickness $r(x, y, z)$ is considered as a field variable for the flow dynamics. At the point when the estimation of mach and the crosses above 0.3 thickness starts to variable and the adequacy of variable spikes when mach number reaches and surpass solidarity, Anderson [4].

The different between Newtonian and non-Newtonian: is that Newtonian fluids have constant viscosity, whereas non-Newtonian fluids have a variable viscosity is the state of being thick and sticky due to the internal friction of the fluid e.g (some liquid such peanut butter, sauce and butter), William *et al.* [52].

Outline of the project

The structure of the project design as follows:

• In Chapter 2, we discuss literature review followed by discussing some explanation of the area of study.

• In Chapter 3, we formulate the mathematical problem.

• In Chapter 4, we transform the PDEs into ODEs

• In Chapter 5, we have the methodology of solution.

• In Chapter 6, we present results and discussion.

• In Chapter 7, conclusion and project outlook.

Chapter 2

Literature Review

Nanofluids are base fluids with nanoparticles suspended in them. Metals, oxides, carbides, and carbon nanotubes are common materials for these nanoparticles. Water, ethyleneglycol, toluene, and oil are some of the most common base fluids. The study of nanofluid flow and stretching sheet has recently gained a lot of attention due to its numerous industrial applications. Polymer extrusion, stretching of plastic films, wire drawing, continuous casting, food and paper manufacturing, glass fiber production, crystal growing, glass blowing, manufacturing of plastic and rubber sheets, and continuous cooling are just a few of these engineering applications Abdelhalim *et al.* [1]. Researchers in fluid dynamics have regularly used fluids in the study of nanofluids during last several decades due to its applications in numerous fields. To improve the heat transfer capability of the fluids, it is necessary to combine both the metal (nano-sized) and fluids. During an investigation of cooling technologies at Argonne National Lab, Choi [10] was the first to establish the notion of nanofluid. There are different types of nanofluids, including environmental process nanofluids, medicinal nanofluids, and extraction nanofluids. The thermal conductivity of nanofluids is affected by particle sizes, particle material, base fluid material, base fluid PH value, temperature, and particle volume concentration. To provide adequate heat transfer increases, nanofluids generally comprise up to 5% volume fraction of nanoparticles. Shagaiya [40] reported the MHD boundary layer slip flow and heat transfer of a permeable sheet. Numerous researchers have conducted numerous experimental and theoretical studies on the thermal conductivity of nanofluids, Khaled *et al.* [23, 25], Yang *et al* [54], Ibrahim and Negera [21], Sudipta and Swati [48].

The field of research in which the magnetic properties of electrically conducting fluids are studied is called magnetohydrodynamics (MHD). Magnetic fluids, liquids, metals and mixtures containing water, salt and other electrolytes are examples of materials that can be investigated via MHD. The MHD is one of the most critical factors in controlling the cooling rate and producing a product of the desired quality. During the past few decades, the study of MHD boundary layer flow on a continuous stretching sheet has received a lot of attention. It has a wide range of uses in industrial manufacturing processes, Dharmendar [13]. The MHD boundary layer flow as a result of an exponentially stretching sheet with radiation effect was discussed, Anuar [6]. Kumaran *et al.* [26] investigated magnetohydrodynamic Casson

and Maxwell flow over a stretching sheet with cross diffusion. Khanba *et al.* [24] conducted MHD boundary layer flow and heat transfer of nanofluids over a nonlinear stretching sheet using the Runge–Kutta–Fehlberg fourth order method. They found out that an increase in Brownian motion parameter and thermophoresis parameter increase the temperature in the thermal boundary layer which consequently reduces the heat transfer rate at the surface.

The study of heat and mass transfer in moving fluids is crucial due to a variety of physical issues, including fluids undergoing exothermic and endothermic chemical reactions. In many chemical engineering processes, chemical reactions take place between a foreign mass and the working fluid which moves due to the stretching of a surface. The order of the chemical reaction depends on several factors. The conveyance of one segment in a mix from a region of high focus to an area of low fixation is called mass transfer. Coupled heat and mass transfer flow create a notable study area in today's fluid flow. Some basic examples are water flow from a lake to the environment, liquor refinement, and so on Goyal *et al.* [17]. The optimal homotopy analysis method (OHAM) and Mathematica package BVPh 2.0 is employed to find a semi-analytical solution. Muriuki [34] examined the MHD flow and heat transfer of a Newtonian fluid moving through parallel porous plates in the presence of an angled magnetic field. Cortell [11] studied the MHD flow and mass transfer of a second-grade electrically conducting fluid in a porous media over a stretching sheet containing chemically reactive species. Other heat and mass transfer can be found in Gnaneswara *et al.* [18], Sudarsana *et al* [49] and Vardya *et al* [51].

The investigation of heat generation or absorption effects is important in cooling processes, which is the main focus of this study. Alsaedi *et al.* [3] studied the effects of heat generation or absorption on nanofluid stagnation point flow over a surface with convective boundary conditions. Mohanty *et al.* [33] studies the chemical reaction effect on MHD Jeffery fluid over a stretching sheet with heat generation/absorption. On MHD stagnation-point flow of a nanofluid over a porous sheet, chemical reactions and uniform heat generation or absorption effects were investigated by Anwar *et al.* [7]. Shateyi *et al.* [43, 45, 47] investigated an unsteady electrically conducting viscous fluid along an infinite vertical permeable plate. Kasmani *et al.* [28] investigated the effect of chemical reaction on boundary layer flow in nanofluid over a wedge with heat generation/absorption and suction on convective heat transfer. Magyaria and Chamkhab [9] studied flow on micropolar fluid flows over a uniformly stretched permeable surface, the combined effect of heat generation or absorption and first-order chemical reaction.

Very recently, Hari *et al.* [30] investigated the effects of chemical reaction and heat generation on MHD Casson fluid flow over an exponentially accelerated vertical plate embedded in a porous medium with ramped wall temperature and ramped surface concentration. Several researchers have focused on MHD boundary layer flow in the last few decades; Mohammed [32], Das [12], and Dodda *et al* [15] have all done work on the topic. The present work follows the direction of the work done by Ferdows *et al.* [16], hence this work has been

modified by including the effects of chemical reaction, heat generation or absorption, buoyancy force thermal expansion and buoyancy force concentration expansion. We compare two recently established approaches by Motsa [35], SLLM and SRM methods on solving the effects of heat generation or absorption and chemical reaction for magnetohydrodynamics boundary layer flow of nanofluid over a stretching sheet. The method relies on converting ODEs into an iterative scheme. The iterative scheme is combined with Chebyshev spectral method, Trefethen [50]. Shateyi and Mukwevho [41], Shateyi [44], and Motsa *et al.* [36] used a similar approach to our current proposed method. The results obtained using the SLLM and SRM methods are compared to those obtained using the Runge Kutta bvp4c matlab inbuilt technique. The purpose of this investigation is to numerically analyze the effects of heat generation or absorption and chemical reaction, boundary layer flow and heat transfer characteristics on the steady MHD of nanofluid over a stretching sheet.

Chapter 3

Mathematical Formulation

The governing equations of the laminar MHD boundary layer flow and heat transfer characteristics of nanofluid over stretching surface are derived. In this chapter we derive equations of continuity equation, momentum equation, energy equation, species concentration equation and also boundary conditions.

3.1 The continuity equation

Conservation law which state that certain physical properties (i.e., measurable quantities) do not change in the course of time within an isolated physical system. Mass inside the control volume is identical to the mass flux crossing the surface S of volume V in essential structure Jiyuan *et al* [22];

$$\frac{d}{dt}\int_V \rho dv = -\int_S \rho \mathbf{u}\cdot\mathbf{n}dS, \tag{3.1.1}$$

where,
- $\mathbf{n}$ - is the outward normal.
- ρ - is density.
- $\mathbf{u}$ - the velocity

The left hand side indicates mass change in the volume V, whereas the right hand side represents in and out flow via the volume's limits. We can take the derivative inside the integral because the volume is fixed in space, and by applying the divergence theorem ($\int_V \nabla.adv = \oint\oint_S a.\mathbf{n}ds$) to the boundary fluxes on the right hand side, we get

$$\int_V \left[\frac{\partial\rho}{\partial t} + \nabla\cdot(\rho\mathbf{u})\right] dv = 0. \tag{3.1.2}$$

If the flow field is smooth, this must hold for any arbitrary volume, no matter how tiny, and so must likewise hold at a point. As a result, the partial differential equation representing mass conservation is:

$$\frac{\partial \rho}{\partial t} + \nabla \cdot (\rho \mathbf{u}) = 0. \tag{3.1.3}$$

By using the definition of the substantial derivative

$$\frac{D()}{Dt} = \frac{\partial()}{\partial t} + \mathbf{u}.\nabla(). \tag{3.1.4}$$

The equation for continuity can be rewritten as

$$\frac{\partial \rho}{\partial t} + \mathbf{u}\nabla\rho + \rho\nabla\mathbf{u}\frac{D\rho}{D\,T} + \rho\nabla\mathbf{u}, \tag{3.1.5}$$

or by using equation (3.1.3) of the mass conservation. In the cartesian coordinate system and can be written as;

$$\frac{\partial \rho}{\partial t} + \frac{\partial(\rho u)}{\partial x} + \frac{\partial(\rho v)}{\partial y} = 0, \tag{3.1.6}$$

where the fluid velocity $\mathbf{u}$ at any point in the flow field is portrayed by nearby velocity components u and v which are in general function of location (x, y) and time (t).
Then we obtain,

$$\frac{\partial \rho}{\partial t} + \rho\left(\frac{\partial u}{\partial y} + \frac{\partial v}{\partial x}\right) = 0, \tag{3.1.7}$$

where,
- $\frac{D\rho}{Dt}$=0 (steady flow) stated as substantial derivative in cartesian coordinates,
- $\frac{D\rho}{Dt}$ is the material derivative
- ρ is the constant total mass density

We obtain the continuity equation as follows;

$$\frac{\partial u}{\partial y} + \frac{\partial v}{\partial x} = 0. \tag{3.1.8}$$

3.2 The momentum equation

Consider the general variable property per unit mass indicated by ϕ, where $\frac{D\phi}{Dt}$ is the substantial derivative of ϕ with respect of time Jiyuan *et al.* [22].

$$\frac{D\phi}{Dt} = \frac{\partial \phi}{\partial t} + u\frac{\partial \phi}{\partial y}, \tag{3.2.1}$$

the above equation characterizes the rate of change of the variable property ϕ per unit mass. The rate of change of the variable property ϕ per unit volume can be acquired by multiplying the density ρ with the considerable derivative of ϕ that is given by,

$$\rho\frac{D\phi}{Dt} = \rho u\frac{\partial\phi}{\partial x} + \rho v\frac{\partial\phi}{\partial y}. \tag{3.2.2}$$

The mass conservation equation derived from equation (3.1.6) defines the sum of the rate change of density and is called the advection term, and can be written as,

$$\frac{\partial\phi}{\partial t} + \frac{\partial(\phi u)}{\partial x} + \frac{\partial(\phi v)}{\partial y} = 0, \tag{3.2.3}$$

the variable property ϕ in conservation form will be ;

$$\frac{\partial(\rho\phi)}{\partial t} + \frac{\partial(\phi u\rho)}{\partial x} + \frac{\partial(\phi v\rho)}{\partial y} = 0, \tag{3.2.4}$$

from above equation (3.2.2) shows the rate of change of ϕ per unit volume with the addition of the net flow of ϕ out of the liquid component per unit volume, illustrate the connection between the moderate type of equation (3.2.4) and nonconservative form of equation (3.2.3), by using the x component of Newton's second law as follows,

$$\Sigma F_x = ma_x. \tag{3.2.5}$$

Where,
- F_x - is force along the x-direction,
- a_x - is acceleration along the x-direction.

The acceleration a_x at the right-hand side of equation (3.2.4) is simple the time rate change of u, which is given by substantial derivative,

$$a_x = \frac{Du}{Dt}, \tag{3.2.6}$$

the mass of the fluid element m is $\rho\Delta x\Delta y\Delta z$, the rate of increase of x-momentum is,

$$\rho\frac{\Delta u}{\Delta t}\Delta x\Delta y. \tag{3.2.7}$$

On the left hand side rule of equation (3.2.7), there are two bases of force that the moving fluid element experiences. The surface force that the velocity component u, that deform the fluid element are due to the normal stress δ_{xx} and tangential stresses yx acting on the surface of the fluid element combining the sum of these surface forces on the fluid element and the time rate change of u from equation (3.2.8) into equation (3.2.6) the x-momentum equation becomes,

$$\rho\frac{Du}{Dt} = \frac{\partial\delta_{xx}}{\partial x} + \frac{\partial\delta_{yx}}{\partial y} + \sum F_x, \tag{3.2.8}$$

where F_x = body force and y-momentum can be obtained as,

$$\rho\frac{Du}{Dt} = \frac{\partial \delta_{xy}}{\partial x} + \frac{\partial \delta_{yy}}{\partial y} + \sum F_y, \tag{3.2.9}$$

where F_y = body force for each structures which can be utilized to express the conservation of a physical quantity for velocity, just nonconservative structure is derived to infer the following physical law known in flow problems. Dividing both equation by ρ, but $\frac{\partial \delta_{xy}}{\partial x} = v\frac{\partial^2 u}{\partial x^2} + v\frac{\partial^2 u}{\partial y^2} + \frac{\partial}{\partial x}\left[\lambda\left(\frac{\partial u}{\partial x} + \frac{\partial u}{\partial y}\right)\right]$ and $\frac{\partial \delta_{yy}}{\partial y} = v\frac{\partial}{\partial x}\left[\frac{\partial u}{\partial x} + \frac{\partial u}{\partial y}\right] + \frac{\partial v}{\partial x}\frac{\partial u}{\partial x} + \frac{\partial v}{\partial y}\frac{\partial v}{\partial x}$, thus equation (3.2.9) become,

$$\frac{Du}{Dt} = -\frac{1}{\rho}\frac{\partial \rho}{\partial x} + v\frac{\partial^2 u}{\partial x^2} + v\frac{\partial^2 u}{\partial y^2} + \frac{\partial}{\partial x}\left[\lambda\left(\frac{\partial u}{\partial x} + \frac{\partial u}{\partial y}\right)\right]$$

$$+v\frac{\partial}{\partial x}\left[\frac{\partial u}{\partial x} + \frac{\partial u}{\partial y}\right] + \frac{\partial v}{\partial x}\frac{\partial u}{\partial x} + \frac{\partial v}{\partial y}\frac{\partial v}{\partial x} + \sum F_x, \tag{3.2.10}$$

and,

$$\frac{Dv}{Dt} = -\frac{1}{\rho}\frac{\partial \rho}{\partial y} + v\frac{\partial^2 v}{\partial x^2} + v\frac{\partial^2 v}{\partial y^2} + \frac{\partial}{\partial y}\left[\lambda\left(\frac{\partial u}{\partial x} + \frac{\partial v}{\partial y}\right)\right]$$

$$+v\frac{\partial}{\partial y}\left[\frac{\partial u}{\partial x} + \frac{\partial v}{\partial y}\right] + \frac{\partial v}{\partial x}\frac{\partial u}{\partial y} + \frac{\partial v}{\partial y}\frac{\partial v}{\partial y} + \sum F_y, \tag{3.2.11}$$

we find that,

$$\frac{Dv}{Dt} = -\frac{1}{\rho}\frac{\partial \rho}{\partial y} + v\frac{\partial^2 v}{\partial x^2} + v\frac{\partial^2 v}{\partial y^2}, \tag{3.2.12}$$

or,

$$\frac{\partial u}{\partial t} + u\frac{\partial u}{\partial x} + v\frac{\partial u}{\partial y} = -\frac{1}{\rho}\frac{\partial \rho}{\partial y} + v\frac{\partial^2 v}{\partial x^2} + v\frac{\partial^2 v}{\partial y^2}, \tag{3.2.13}$$

and,

$$\frac{\partial v}{\partial t} + u\frac{\partial v}{\partial x} + v\frac{\partial v}{\partial y} = -\frac{1}{\rho}\frac{\partial \rho}{\partial y} + v\frac{\partial^2 u}{\partial x^2} + v\frac{\partial^2 u}{\partial y^2}. \tag{3.2.14}$$

If the time independent term $\frac{\partial v}{\partial t} = 0$, $\frac{\partial^2 u}{\partial x^2} = \frac{\partial U}{\partial x}$ and $\frac{1}{\rho}\frac{\partial \rho}{\partial y} = \frac{\sigma B_o^2 (U-u)}{\rho}$ we get

$$u\frac{\partial u}{\partial x} + v\frac{\partial u}{\partial y} = U\frac{\partial U}{\partial x} + v\frac{\partial^2 u}{\partial y^2} + \frac{\sigma B_o^2}{\rho}(U-u). \tag{3.2.15}$$

3.3 The energy equation

The equation of conservation of energy which has been derived from consideration of the first law of thermodynamics Jiyuan *et al* [22];

$$\begin{pmatrix} Time\ rate\ of \\ change\ of\ energy \end{pmatrix} = \begin{pmatrix} Net\ rate\ of \\ heat\ added \end{pmatrix} \left(\sum \dot{Q}\right) + \begin{pmatrix} Net\ rate\ of \\ work\ done \end{pmatrix} \left(\sum \dot{W}\right), \tag{3.3.1}$$

where $\sum \dot{Q}$ is heat added to the system from surroundings and $\sum \dot{W}$ workdone by the system on its surroundings. The time rate of change in energy for the moving fluid element is simplified as,

$$\rho \frac{D\varepsilon}{D\tau} \Delta x \Delta y, \tag{3.3.2}$$

when we put together all the inputs of the surface forces in the x and y directions and substituting these expressions along with the time rate change of energy E, from equation (3.3.1) into (3.3.2) the equation for the conservation of energy can be written as,

$$\rho \frac{DE}{Dt} = \frac{\partial \tau_{xx}}{\partial x} + \frac{\partial \tau_{yy}}{\partial y} + \frac{\partial \tau_{yx}}{\partial y} + \frac{\partial \tau_{xy}}{\partial x} + \frac{\partial q_x}{\partial x} + \frac{\partial q_y}{\partial y}, \tag{3.3.3}$$

the energy fluxes q_x and q_y equation (3.3.3) can be expressed by applying Fourier's law of the heat conduction that relates flux to the local temperature gradient,

$$q_x = -k \frac{\partial T}{\partial x} \text{ and } q_y = -k \frac{\partial T}{\partial y}, \tag{3.3.4}$$

where k given as the thermal conductivity, substitute equation (3.3.4) into equation (3.3.3), applying the normal stresses and the energy equation is as follows;

$$\rho \frac{DE}{Dt} = \frac{\partial}{\partial x}\left[k \frac{\partial T}{\partial x}\right] + \frac{\partial}{\partial y}\left[k \frac{\partial T}{\partial y}\right] - \frac{\partial (up)}{\partial x} - \frac{\partial (vp)}{\partial y} + \varphi, \tag{3.3.5}$$

the effects expected viscous stresses of the energy equation are written as,

$$\phi = \frac{\partial (u\tau_{xx})}{\partial x} + \frac{\partial \tau_{yy}}{\partial y} + \frac{\partial (u\tau_{yx})}{\partial y} + \frac{\partial (v\tau_{xy})}{\partial x}, \tag{3.3.6}$$

where the fluid is assumed to be incompressible, the continuity equation applies by neglecting, the enthalph(thermodynamic system, is equal to the system is internal energy plus the product of its pressure), the kinetic energy can be reduced to C_pT where C_p is the specific heat and is assumed to be constant, equation (3.3.5) can be written follows,

$$\rho C_p \frac{DT}{Dt} = \frac{\partial}{\partial x}\left[k \frac{\partial T}{\partial x}\right] + \frac{\partial}{\partial y}\left[k \frac{\partial T}{\partial y}\right] + \frac{\partial p}{\partial x} + \varphi, \tag{3.3.7}$$

in most functional liquid engineering complications, the local time derivative of pressure $\frac{\partial p}{\partial t}$ and the dissipation function ϕ can be left out and equation (3.3.7) reduce as,

$$\rho C_p \frac{DT}{Dt} = \frac{\partial}{\partial x}\left[k\frac{\partial T}{\partial x}\right] + \frac{\partial}{\partial y}\left[k\frac{\partial T}{\partial y}\right], \tag{3.3.8}$$

expecting that the temperature which invariant along the y-direction and the thermal conductivity is constant, then the equation for the conservation of energy in two-measurements can be written as,

$$\frac{\partial T}{\partial t} + u\frac{\partial T}{\partial x} + v\frac{\partial T}{\partial y} = \frac{k}{\rho C_\rho}\frac{\partial^2 T}{\partial x^2} + \frac{k}{\rho C_\rho}\frac{\partial^2 T}{\partial y^2}, \tag{3.3.9}$$

time independent $\frac{\partial T}{\partial t} = 0$ by using continuity equation $\frac{\partial u}{\partial x} + \frac{\partial v}{\partial y} = 0$, then consider the fact that $\frac{\partial^2 T}{\partial x^2} << \frac{\partial^2 T}{\partial y^2}$, $\alpha = \frac{k}{\rho}$ and $\frac{k}{\rho c_\rho}(\frac{\partial^2 T}{\partial x^2}) = \alpha\frac{\partial^2 T}{\partial y^2} - \frac{\alpha}{k}\frac{\partial q_r}{\partial y}$

$$u\frac{\partial T}{\partial x} + v\frac{\partial T}{\partial y} = \alpha\frac{\partial^2 T}{\partial y^2} - \frac{\alpha}{k}\frac{\partial q_r}{\partial y} + \frac{\alpha}{c_p}\left(\frac{\partial u}{\partial y}\right)^2 + \tau\left(D_B\frac{\partial T}{\partial y}\frac{\partial C}{\partial y} + \frac{D_T}{T_\infty}\left(\frac{\partial T}{\partial y}\right)^2\right)$$

$$\pm\frac{Q}{\rho c_\rho}(T - T_\infty). \tag{3.3.10}$$

3.4 Derivation of the species equation

The pertinent form of the conservation equation can be obtained by identifying the processes that affect the transport and generation of species B for a differential control volume in the fluid, Wongwise [53].

Species B can be moved in each of the coordinate directions by advection (with the mixture's mean velocity) and diffusion (relative to the mean motion). The concentration may also be affected by chemical reactions, and we designate the rate at which the mass of species A is generated per unit volume due to such reactions as $\dot{n}$. The net rate for which species (B) enters the control volume due to advection in the x-direction is,

$$\dot{M}_{B,bdv,x} - \dot{M}_{B,bdv,x+dx} = (\rho_B u)dy - \left[(\rho_B u) + \frac{\partial(\rho_B u)}{\partial x}dx\right]dy \tag{3.4.1}$$

$$= \frac{\partial(\rho_B u)}{\partial x}dxdy. \tag{3.4.2}$$

- $\dot{M}_B$ is the molecular weight in (kg/kmol).

Similarly, the net rate at which species (C) enters the control volume due to diffusion in the x-direction is calculated by multiplying both sides of Fick's equation (Equation 3.4.2) by the

molecular weight $(B)\mu(kg/kmol)$ of species A.

$$\begin{aligned}\dot{M}_{B,dif,x} - \dot{M}_{B,dif,x+dx} &= \left(-D_{BC}\frac{\partial \rho_B u}{\partial x}\right)dy - \left[\left(-D_{BC}\frac{\partial \rho_B}{\partial x}\right) + \frac{\partial}{\partial x}\left(-D_{BC}\frac{\partial \rho_B}{\partial x}\right)dx\right]dy \\ &= \frac{\partial}{\partial x}\left(D_{BC}\frac{\partial \rho_B}{\partial x}\right)dxdy. \qquad (3.4.3)\end{aligned}$$

For the y-direction, expressions similar to Equations (3.4.2) and (3.4.3) can be used.

$$\dot{M}_{B,bdv,x} - \dot{M}_{B,bdv,x+dx} + \dot{M}_{B,bdv,y} - \dot{M}_{B,bdv,y+dy} + \dot{M}_{B,dif,x} - \dot{M}_{B,dif,x+dx}$$

$$+\dot{M}_{B,dif,x} - \dot{M}_{B,dif,x+dx} - \dot{M}_{B,dif,y+dy} + \dot{M_{B,g}} = 0, \qquad (3.4.4)$$

by substituting equations (3.4.2) and (3.4.3) and as well as from similar form for the y-direction, we get the following:

$$\frac{\partial\left(\rho_B u\right)}{\partial x} + \frac{\partial(\rho_B v)}{\partial y} = \frac{\partial}{\partial x}\left(D_{BC}\frac{\partial \rho_B}{\partial x}\right) + \frac{\partial}{\partial y}\left(D_{BC}\frac{\partial \rho_B}{\partial x}\right) + \dot{n}_B. \qquad (3.4.5)$$

This equation is obtained by expanding the terms on the left-hand side and substituting from the overall continuity equation for an incompressible fluid. The equation (3.4.5) is reduced to

$$u\frac{\partial \rho_B}{\partial x} + v\frac{\partial \rho_B}{\partial y} = \frac{\partial}{\partial x}\left(D_{BC}\frac{\partial \rho_B}{\partial x}\right) + \frac{\partial}{\partial y}\left(D_{BC}\frac{\partial \rho_B}{\partial y}\right) + \dot{n}_B, \qquad (3.4.6)$$

or put it in a molar form :

$$u\frac{\partial C_B}{\partial x} + v\frac{\partial C_B}{\partial y} = \frac{\partial}{\partial x}\left(D_{BC}\frac{\partial C_B}{\partial x}\right) + \frac{\partial}{\partial y}\left(D_{BC}\frac{\partial C_B}{\partial y}\right) + \dot{N}_B, \qquad (3.4.7)$$

by replacing $\dot{N}_B = -K_o(C - C_\infty)$, $\frac{\partial}{\partial x}\left(D_{BC}\frac{\partial C_B}{\partial x}\right) = D_B\frac{\partial^2 C}{\partial y^2}$ and $\frac{\partial}{\partial y}(D_{BC}\frac{\partial C_B}{\partial x}) = \frac{D_T}{T_\infty}\left(\frac{\partial^2 T}{\partial y^2}\right)$

$$u\frac{\partial C}{\partial x} + v\frac{\partial C}{\partial y} = D_B\frac{\partial^2 C}{\partial y^2} + \frac{D_T}{T_\infty}\left(\frac{\partial^2 T}{\partial y^2}\right) - K_o(C - C_\infty). \qquad (3.4.8)$$

3.5 Derivation of boundary conditions

For this research, a steady two-dimensional boundary layer flow of a nanofluid toward stretching sheet is considered. A linearly variation of $u_w = ax$ with the distance x, where a is constant and x is the coordinate measured along the stretching surface. The flow considered to be laminar, incompressible, Newtonian and electrically conducting fluid. Steady uniform stress leading to equal and opposite is applied along the x-axis so that the sheet is stretching keeping the origin fixed. The electrical field is assumed to be zero and both the induced magnetic and electric field of the flow are insignificant compared with the small Reynolds number and $U = bx$ where U is considered to magnetic field and b is constant. The temperature and concentration of the ambient fluid are T_∞ and C_∞, the stretching sheet surface is maintained at a uniform temperature T_w and concentration C_w respectively. The boundary condition for velocity component, temperature and concentration of nanofluid, therefore can be given as follows;

$$v = 0,\ u = ax,\ C = C_w = C_\infty + A_2\left(\frac{x}{l}\right)^m,\ T = T_w = T_\infty + A_1\left(\frac{x}{l}\right)^m \text{ at } y = 0$$

$$T = T_\infty,\ C = C_\infty,\ U = bx \text{ as } y \to \infty. \tag{3.5.1}$$

Where A_1, A_2 are constant whose values depend on the properties of the fluid T_∞ temperature of the ambient fluid, subscript ∞ indicate the condition at the outer edge of the boundary layer, and λ is linear stretching constant parameter.

3.6 Physical model of the problem

We consider a steady two-dimensional magnetohydrodynamics boundary layer flow of nanofluid over a stretching sheet in the presence of heat generation or absorption, as well as a variation in chemical reaction velocity with distance $u_w = ax$. The flow is described as laminar, incompressible, electrically conducting, and Newtonian, with x representing the coordinate measured along the stretching surface and a representing a constant. The coordinate of a constant uniform stress resulting in equal and opposite forces is applied along the x-axis to stretch the sheet while keeping the origin constant. Ferdows *et al.* [16] provides an approximation of the governing boundary layer equations for continuity, momentum, energy, and concentration based on the above assumptions:

$$\frac{\partial u}{\partial x} + \frac{\partial v}{\partial y} = 0, \tag{3.6.1}$$

$$u\frac{\partial u}{\partial x} + v\frac{\partial v}{\partial y} = U\frac{dU}{dx} + v\frac{\partial^2 v}{\partial y^2} + \frac{\sigma B_o^2}{\rho}(U - u) + g\beta_t(T_w - T_\infty) + G\beta_c(C_w - C_\infty), \tag{3.6.2}$$

$$u\frac{\partial T}{\partial x}+v\frac{\partial T}{\partial y}=\alpha\frac{\partial^2 T}{\partial y^2}-\frac{\alpha}{k}\frac{\partial q_r}{\partial y}+\frac{\alpha}{c_\rho}\left(\frac{\partial u}{\partial y}\right)^2+\tau\left\{D_B\frac{\partial T}{\partial y}\frac{\partial C}{\partial y}+\frac{D_T}{T_\infty}\left(\frac{\partial T}{\partial y}\right)^2\right\}$$

$$\pm\frac{Q}{\rho c_\rho}(T-T_\infty), \tag{3.6.3}$$

$$u\frac{\partial C}{\partial x}+v\frac{\partial C}{\partial y}=D_B\frac{\partial^2 C}{\partial y^2}+\frac{D_T}{T_\infty}\left(\frac{\partial^2 T}{\partial y^2}\right)-K_o(C-C_\infty). \tag{3.6.4}$$

Where u and v are the fluid velocity components along x and y axes, respectively, U represents the plate velocity (uniform velocity), c_ρ represents the specific heat at constant pressure, ρ represents the density of the fluid, q_r represents the radiation heat flux, τ represents the Stefan-Boltzmann constant, B_o represents externally imposed magnetic field strength in the y direction, D_B represents the Brownian diffusion coefficient, D_T represents the thermophoresis diffusion coefficient, k represents the thermal, α represents the thermal diffusivity, T_w represents the temperature of the wall, T and C are the fluid's local temperature and concentration, T_∞ and C_∞ are the ambient fluid's temperature and concentration, K_o is the chemical reaction parameter and Q is the heat generation/absorption coefficient with boundary conditions.

$$v=0,\ u=ax,\ C=C_w=C_\infty+A_2\left(\frac{x}{l}\right)^m,\ T=T_w=T_\infty+A_1\left(\frac{x}{l}\right)^m \text{ at } y=0,$$

$$T=T_\infty,\ C=C_\infty,\ U=bx \text{ as } y\to\infty. \tag{3.6.5}$$

Where A_1, A_2 are constants whose values are determined by the fluid properties, a and b are linear stretching constants, l is the characteristic length m is constant parameter.

Chapter 4

Transformation Techniques

In this chapter, we focus on similarity transformations, whereby the stream function and stretching sheet velocity are defined. Then governing non-linear PDEs are converted into non-linear ODEs then transformed into continuity, linear momentum, energy, species concentration equation and the quantities of physical interest, Jiyuan *et al* [22].

4.1 Stream function and dimensionless variable

The stream function is $\psi(x,y)$ such that $u=\frac{\partial\psi}{\partial y}$ and $v=-\frac{\partial\psi}{\partial x}$ satisfies the equations (3.6.1 - 3.6.4).

$$\psi = x\sqrt{av}f(\eta), \quad \eta = y\sqrt{\frac{a}{v}}. \tag{4.1.1}$$

$$\theta = \frac{T-T_\infty}{T_w-T_\infty} \Longrightarrow T = \theta(T_w-T_\infty)+T_\infty, \tag{4.1.2}$$

$$\phi = \frac{C-C_\infty}{C_w-C_\infty} \Longrightarrow C = \phi(C_w-C_\infty)+C_\infty, \tag{4.1.3}$$

firstly, we derive the transformed variable η with respect to $(x,\ y)$ respectively as follows;

$$\eta = \frac{\partial\eta}{\partial y} = \sqrt{\frac{a}{v}}, \qquad \eta = \frac{\partial\eta}{\partial x} = 0, \tag{4.1.4}$$

the y-direction for u velocity,

$$u = \frac{\partial\psi}{\partial y} = u = x\mathrm{a}f'(\eta), \tag{4.1.5}$$

the x-direction for v velocity,

$$\nu = -\frac{\partial \psi}{\partial x} = -\sqrt{a\upsilon} f(\eta), \tag{4.1.6}$$

the Rosseland approximation have been considered for radiative heat flux leads to;

$$q_r = \frac{4\sigma}{3k^*}\frac{\partial T^4}{\partial y}, \tag{4.1.7}$$

where k^* is the mean absorption coefficient, q_r is radiative heat flux. σ is Stefan-Boltzmann constant and we can obtain T^4 by expanding in a Taylor series about T_∞ and neglecting the higher order term, we get;

$$T^4 = T_\infty^4 + (T - T_\infty) f'(T_\infty) + \frac{(T - T_\infty)^2}{2!} f''(T_\infty)$$

$$+ \frac{(T - T_\infty)^3}{3!} f'''(T_\infty) + \frac{(T - T_\infty)^4}{4!} f''''(T_\infty) + ...$$

$$T^4 + 4TT_\infty^3 - 4TT_\infty^4 + 6TT_\infty^2 + 6TT_\infty^2(T^3 - 3T^2T_\infty - T_\infty^3) +$$

$$= 4TT_\infty^3 - 3T_\infty^4, \tag{4.1.8}$$

so then radiation term in energy equation take a form,

$$\frac{\partial q_r}{\partial y} = \frac{16\sigma T_\infty^3}{3k^*}\frac{\partial^2 T}{\partial y^2}. \tag{4.1.9}$$

4.2 Similarity transformation of the continuity equation

Consider the function for u and v velocity components :

$$u = axf'(\eta), \qquad v = -\sqrt{a\upsilon} f(\eta), \tag{4.2.1}$$

then we compute equation (4.2.1) using partial derivative as follows:

$$\frac{\partial u}{\partial x} = af' + axf''\frac{\partial \eta}{\partial x} = af', \qquad \frac{\partial v}{\partial y} = -\sqrt{a\upsilon} f'(\eta)\sqrt{\frac{a}{\upsilon}} = -af'. \tag{4.2.2}$$

Therefore, we substitute equations (4.2.1) and (4.2.2) into (3.6.1) to obtain;

$$\frac{\partial u}{\partial x} + \frac{\partial \nu}{\partial y} = 0 \Rightarrow af' - af' = 0. \tag{4.2.3}$$

The continuity equation is satisfied.

4.3 Similarity transformation of the linear momentum equation

We use similarity transformation of momentum equation to reduce non-linear equation (3.6.2) coupled ODEs by dimensionless variable,

$$u\frac{\partial u}{\partial x}+v\frac{\partial v}{\partial y}=U\frac{dU}{dx}+v\frac{\partial^2 v}{\partial y^2}+\frac{\sigma B_o^2}{\rho}(U-u)+g\beta_t(T_w-T_\infty)+G\beta_c(C_w-C_\infty). \tag{4.3.1}$$

We compute from equation (4.2.2) and $U=bx$ using partial derivative to form;

$$\frac{\partial u}{\partial x}=af', \qquad \frac{\partial u}{\partial y}=ax\sqrt{\frac{a}{\upsilon}}f'', \tag{4.3.2}$$

$$\Rightarrow \frac{\partial^2 u}{\partial y^2}=\frac{a^2}{\upsilon}xf''', \qquad \frac{\partial U}{\partial x}=b, \tag{4.3.3}$$

$$\tag{4.3.4}$$

$$g\beta_t(T_w-T_\infty)=g\beta_t(T_\infty+\theta(T_w-T_\infty)-T_\infty)=g\theta\beta_t(T_w-T_\infty), \tag{4.3.5}$$

$$G\beta_c(T_w-T_\infty)=G\beta_c(C_\infty+\phi(C_w-C_\infty)-C_\infty)=G\phi\beta_c(C_w-C_\infty), \tag{4.3.6}$$

by substituting (4.3.2), (4.3.3), (4.3.4) and (4.3.5) into (4.3.1) we have,

$$axf'af'+\sqrt{a\upsilon}fa\sqrt{\frac{a}{\upsilon}}f''=bx*b+v\frac{a^2}{\upsilon}xf'''+\frac{\sigma B_o^2}{\rho}(bx-axf')$$

$$+g\theta\beta_t(T_w-T_\infty)+G\phi\beta_c(C_w-C_\infty), \tag{4.3.7}$$

then after substituting we get,

$$a^2xf'^2-a^2xff''=b^2x+a^2xf'''+\frac{\sigma B_o^2}{\rho}(bx-axf')+G_t\theta+G_c\phi, \tag{4.3.8}$$

divide the equation by a^2x both sides and given that $\lambda=\frac{b}{a}$ so we have,

$$f'^2-ff''=\lambda^2+f'''+\frac{\sigma B_o^2}{a\rho}(\lambda-f')\,G_t\theta+G_c\phi, \tag{4.3.9}$$

setting $M=\frac{\sigma B_o^2}{a\rho}$ the magnetic parameter, β_t is thermal expansion coefficient, β_c is concentration expansion coefficient, g is gravitational acceleration, $C_{_w}$ is concentration along the stretching sheet and C_∞ ambient concentration.

Therefore,

$$f'''+ff''-f'^2+M(\lambda-f')+\lambda^2+G_t\theta+G_c\phi=0. \tag{4.3.10}$$

4.4 Similarity transformation of the energy equation

We use similarity transformation of energy equation to reduce equation (3.6.3) to non-linear coupled ODEs by dimensionless variable,

$$u\frac{\partial T}{\partial x}+\nu\frac{\partial T}{\partial y}=\alpha\frac{\partial^2 T}{\partial y^2}-\frac{\alpha}{k}\frac{\partial q_r}{\partial y}+\frac{\alpha}{c_p}\left(\frac{\partial u}{\partial y}\right)^2+\tau\left(D_B\frac{\partial T}{\partial y}\frac{\partial C}{\partial y}+\frac{D_T}{T_\infty}\left(\frac{\partial T}{\partial y}\right)^2\right)$$

$$\pm\frac{Q}{\rho c_\rho}(T-T_\infty). \tag{4.4.1}$$

We compute equations (4.1.2), (4.1.3) of nanofluid and (4.1.9) using partial derivative this form;

$$\frac{\partial T}{\partial y}=\sqrt{\frac{a}{\nu}}\theta'(T_w-T_\infty)\Rightarrow\frac{\partial^2 T}{\partial y^2}=\frac{a}{v}(T_w-T_\infty)\theta'',\qquad\frac{\partial C}{\partial y}=\phi'\sqrt{\frac{a}{\mu}}(C_w-C_\infty), \tag{4.4.2}$$

we use boundary condition (3.6.5) to derive partial derivative this form;

$$T=T_w=T_\infty+A_1\left(\frac{x}{l}\right)^m\theta\Rightarrow T=T_w=T_\infty+A_1\left(\frac{x}{l}\right)^m\theta,$$

$$\Rightarrow\frac{\partial C}{\partial x}=mA_1\left(\frac{x}{l}\right)^{m-1}\theta, \tag{4.4.3}$$

$$u\frac{\partial T}{\partial x}=axf'mA_1\left(\frac{x}{l}\right)^{m-1}\theta, \tag{4.4.4}$$

$$v\frac{\partial T}{\partial y}=\sqrt{av}f\sqrt{\frac{a}{\upsilon}}\left(T_w-T_\infty\right)\theta'=-af\theta'\left(T_w-T_\infty\right), \tag{4.4.5}$$

$$\alpha\frac{\partial^2 T}{\partial y^2}=\alpha\frac{a}{\upsilon}\left(T_w-T_\infty\right)\theta'', \tag{4.4.6}$$

$$\frac{\alpha}{k}\frac{\partial q_r}{\partial y}=-\frac{16\sigma\alpha T_\infty^3}{3kk^*}\frac{\partial^2 T}{\partial y^2}=-\frac{16\sigma\alpha T_\infty^3}{3kk^*}\frac{a}{\upsilon}\left(T_w-T_\infty\right)\theta'', \tag{4.4.7}$$

$$\frac{\alpha}{c_\rho}\left(\frac{\partial u}{\partial y}\right)^2=\frac{\alpha a^3x^2f''^2}{\upsilon c_\rho}, \tag{4.4.8}$$

$$D_B \frac{\partial T}{\partial y}\frac{\partial C}{\partial y} = D_B \sqrt{\frac{a}{\upsilon}}\left(T_w - T_\infty\right)\sqrt{\frac{a}{\upsilon}}\left(C_w - C_\infty\right)\phi'\theta'$$

$$= D_B \frac{a}{\upsilon}\left(T_w - T_\infty\right)\left(C_w - C_\infty\right)\phi'\theta', \tag{4.4.9}$$

$$\frac{D_T}{T_\infty}\left(\frac{\partial T}{\partial y}\right)^2 = \frac{D_T}{T_\infty}\left(\sqrt{\frac{a}{\upsilon}}\left(T_w - T_\infty\right)\theta'\right)^2 = \frac{D_T}{T_\infty}\frac{a}{\upsilon}\left(T_w - T_\infty\right)^2\theta'^2$$

$$\frac{Q}{\rho c_\rho}\left(T - T_\infty\right) = \frac{Q}{\rho c_\rho}\left(T_w - T_\infty\right)\theta, \tag{4.4.10}$$

by substituting (4.4.4), (4.4.5), (4.4.6), (4.4.7), (4.4.8), (4.4.9), (4.4.10) and (4.4.11) into (4.4.1) we have,

$$axf'mA_1\left(\frac{x}{l}\right)^{m-1}\theta - af\theta'\left(T_w - T_\infty\right) = \alpha\frac{a}{\upsilon}\left(T_w - T_\infty\right)\theta'' + \frac{16\sigma\alpha T_\infty^3}{3kk^*}\frac{a}{\upsilon}\left(T_w - T_\infty\right)\theta'' + \frac{\alpha a^3x^2f''^2}{\upsilon c_\rho}$$

$$+D_B\frac{a}{\upsilon}\left(T_w - T_\infty\right)\left(C_w - C_\infty\right)\phi'\theta' + \frac{D_T}{T_\infty}\frac{a}{\upsilon}\left(T_w - T_\infty\right)^2\theta'^2 \pm \frac{Q}{\rho c_\rho}\left(T_w - T_\infty\right)\theta, \tag{4.4.11}$$

divide the equation (4.4.12) by $\frac{a\alpha(T_w - T_\infty)}{\upsilon}$ both sides, we have,

$$\frac{mA_1(\frac{x}{l})^{m-1}axf'\upsilon}{a\alpha(T_w - T_\infty)} - \frac{\upsilon}{\alpha}f\theta' = (1 + \frac{16\sigma\alpha T^3}{3kk^*})\theta'' + \frac{\alpha a^2x^2f''^2}{\left(T_w - T_\infty\right)c_\rho} + \frac{D_B}{\alpha}\left(C_w - C_\infty\right)\phi'\theta'$$

$$+\frac{D_T}{T_\infty}\left(T_w - T_\infty\right)\theta'^2 \pm \frac{\upsilon}{\alpha}\frac{Q}{\rho c_\rho a}\theta, \tag{4.4.12}$$

where $Pr = \frac{\upsilon}{\alpha}$ is Prandtl number, T_w is the temperature of the wall and, T_∞ is the temperature, $l = \sqrt{\frac{\upsilon}{a}}$ is a characteristics length, $R = \frac{16\sigma\alpha T^3}{3kk^*}$ is radiation parameter, A depends on the thermal properties of the liquid, $Ec = \frac{\alpha a^2x^2}{(T_w - T_\infty)c_\rho}$ is the Eckert number, $D_B = \frac{\upsilon Nb(\rho c(C_w - C_\infty))_f}{(\rho c)_\rho}$ is the Brownian diffusion coefficient, $D_T = \frac{\upsilon Nt(\rho c)_f(T_w - T_\infty)}{(\rho c)_\rho}$ is the thermophoresis diffusion coefficient, $u_w = ax$ is the linear velocity and $S = \frac{Q}{\rho c_\rho a}$ is the heat generation parameter. Substituting the explained parameters above into equation (4.4.13), we get:

$$mf'\theta\frac{A_1(\frac{x}{l})^m\upsilon}{\alpha(T_w - T_\infty)} - Prf\theta' = (1 + R)\theta'' + Ecf''^2 + \frac{\upsilon\cdot\upsilon\ Nb(\rho c)_f\left(C_w - C_\infty\right)}{\alpha(\rho c)_\rho}\phi'\theta' +$$

$$\frac{\upsilon\cdot\upsilon\ Nt(\rho c)_f\left(T_w - T_\infty\right)}{\alpha(\rho c)_\rho}\theta'^2 - mf'\theta Pr\frac{\left(T_w - T_\infty\right)}{\left(T_w - T_\infty\right)} \pm \frac{\upsilon}{\alpha}\frac{Q}{\rho c_\rho a}\theta, \tag{4.4.13}$$

hence the energy is given,

$$(1 + R)\theta'' + EcPrf''^2 + Prf\theta' - mPrf'\theta + PrNb\phi'\theta' + PrNt\theta'^2 \pm PrS\theta = 0. \tag{4.4.14}$$

4.5 Similarity transformation of the concentration equation

We use similarity transformation of concentration equation to reduce non-linear equation (3.6.4) coupled ODEs by dimensionless variable,

$$u\frac{\partial C}{\partial x}+\nu\frac{\partial C}{\partial y}=D_B\frac{\partial^2 C}{\partial y^2}+\frac{D_T}{T_\infty}\left(\frac{\partial^2 T}{\partial y^2}\right)-K_o(C-C_\infty). \tag{4.5.1}$$

The transformed derived equations (4.1.2) and (4.1.3) are as follows;

$$C=C_w=C_\infty+A_2\left(\frac{x}{l}\right)^m\phi\Rightarrow, C=C_w=C_\infty+A_2\left(\frac{x}{l}\right)^m\phi,$$

$$\Rightarrow\frac{\partial C}{\partial x}=mA_2\left(\frac{x}{l}\right)^{m-1}\phi, \tag{4.5.2}$$

$$u\frac{\partial C}{\partial x}=axf'mA_2\left(\frac{x}{l}\right)^{m-1}\phi, \tag{4.5.3}$$

$$\nu\frac{\partial C}{\partial y}=-af\phi'(C_w-C_\infty), \tag{4.5.4}$$

$$D_B\frac{\partial^2 C}{\partial y^2}=D_B\frac{a}{\upsilon}(C_w-C_\infty)\phi'', \tag{4.5.5}$$

$$\frac{D_T}{T_\infty}\left(\frac{\partial^2 T}{\partial y^2}\right)=\frac{D_T}{T_\infty}\frac{a}{\upsilon}\theta''(T_w-T_\infty), \tag{4.5.6}$$

$$k(C-C_\infty)=-K_o(C_w-C_\infty)\phi, \tag{4.5.7}$$

by substituting (4.5.2), (4.5.3), (4.5.4), (4.5.5), ((4.5.6), (4.5.7) and (4.4.11) into (4.5.1) we have,

$$axmA_2\left(\frac{x}{l}\right)^{m-1}f'\phi-af\phi'(C_w-C_\infty)=D_B\frac{a}{\upsilon}\phi''(C_w-C_\infty)$$

$$+\frac{D_T}{T_\infty}\frac{a}{\upsilon}\theta''(T_w-T_\infty)-K_o(C_w-C_\infty)\phi, \tag{4.5.8}$$

divide the equation (4.5.8) by $\frac{axD_B(C_w-C_\infty)}{\upsilon}$ both sides, we have,

$$\phi'' + \frac{\upsilon}{D_B} f\phi' + \frac{D_T T_\infty}{D_B}\frac{T_w - T_\infty}{C_w - C_\infty}\theta'' - \gamma\frac{xu_w}{\upsilon}\frac{\upsilon}{D_B}\phi - mf'\phi\frac{A_2(\frac{x}{l})^{m-1}}{a\,(C_w - C_\infty)}\frac{\upsilon}{D_B} = 0, \tag{4.5.9}$$

$$\phi'' + \frac{\upsilon}{D_B} f\phi' + \frac{D_T T_\infty}{D_B}\frac{T_w - T_\infty}{C_w - C_\infty}\theta'' - \gamma\frac{xu_w}{\upsilon}\frac{\upsilon}{D_B}\phi - mf'\phi\frac{\upsilon}{D_B}\frac{A_2(\frac{x}{l})^{m}\frac{x}{l}^{-1}}{C_w - C_\infty} = 0, \tag{4.5.10}$$

$$\phi'' + \frac{\upsilon}{D_B} f\phi' + \frac{D_T T_\infty}{D_B}\frac{T_w - T_\infty}{C_w - C_\infty}\theta'' - \gamma\frac{xu_w}{\upsilon}\frac{\upsilon}{D_B}\phi - mf'\phi\frac{\upsilon}{D_B}\frac{C_w - C_\infty}{C_w - C_\infty} = 0, \tag{4.5.11}$$

where T_w is temperature of the wall, T_∞ is temperature, $l = \sqrt{\frac{\upsilon}{a}}$ is a characteristics length, A depends on the thermal properties of the liquid, $K_o = \frac{\gamma U_w^2}{\upsilon}$ is the reaction parameter, D_T is thermophoresis diffusion coefficient, $Re_x = \frac{xu}{\upsilon}$ is the local Reynolds number, $Le = \frac{\upsilon}{D_B}$ is Lewis number, Nt is thermophoresis parameter, m is constant, $N_{bt} = \frac{D_T T_\infty}{D_B}\frac{T_w - T_\infty}{C_w - C_\infty} = \frac{Nt}{Nb}$ where Nb is Brownian motion parameter, D_B is Brownian diffusion coefficient. Substituting the explained parameters above into equation (4.5.11), we have

$$\phi'' + Lef\phi' + N_{bt}\theta'' - \gamma Re_x Le\phi - mLef'\phi = 0, \tag{4.5.12}$$

therefore the concentration is given,

$$\phi'' + Lef\phi' + \frac{Nt}{Nb}\theta'' - \gamma Re_x Le\phi - mLef'\phi = 0, \tag{4.5.13}$$

or,

$$\phi'' + Lef\phi' + \frac{Nt}{Nb}\theta'' - Le\phi(\gamma Re_x + mf') = 0. \tag{4.5.14}$$

4.6 Similarity transformation of boundary condition

Our boundary conditions are transformed using the simulation $u = \frac{\partial\psi}{\partial y}$, $v = \frac{\partial\psi}{\partial x}$ and $\psi = \sqrt{a\nu}xf(\eta)$, we get $u = axf'(\eta)$ and $v = -\sqrt{\nu}f(\eta)$ from (4.1.1), $u = u_w(x) = ax$ is a stretching velocity with $(a > 0)$ being the stretching constant, (Re_x) is local Reynolds number and $y = 0$ together with $T \to T_\infty$ and $C \to C_\infty$ now we can derive boundary condition as follows;

when $y = 0$,

$$u = axf',\ ax = axf' \Rightarrow f'(0) = \frac{ax}{ax} = 1, \tag{4.6.1}$$

then,

$$v = -\sqrt{a\nu}f,\ 0 = -\sqrt{a\nu}f \Rightarrow f(0) = 0, \tag{4.6.2}$$

$$T = T_w = T_\infty + A_1\left(\frac{x}{l}\right)^m,\ \text{then we have}\ \ \theta(0) = \frac{T - T_\infty}{T_w - T_\infty} = \frac{T_\infty + A_1(\frac{x}{l})^m}{T_\infty + A_1(\frac{x}{l})^m} = 1, \tag{4.6.3}$$

$$C = C_w = C_\infty + A_1\left(\frac{x}{l}\right)^m,\ \text{then we have}\ \phi(0) = \frac{C - C_\infty}{C_w - C_\infty} = \frac{C_\infty + A_1(\frac{x}{l})^m}{C_\infty + A_1(\frac{x}{l})^m} = 1, \tag{4.6.4}$$

and we solve at $y \to \infty$,

$$u = axf', \tag{4.6.5}$$

$$bx = axf' \Rightarrow f'(\infty) = \frac{bx}{ax} = \frac{b}{a} = \lambda, \tag{4.6.6}$$

$$T \to T_\infty,\ \theta(\infty) = \frac{T - T_\infty}{T_w - T_\infty} \Rightarrow \theta(\infty) = \frac{T_\infty - T_\infty}{T_w - T_\infty} = 0, \tag{4.6.7}$$

therefore,

$$C \to C_\infty,\ \theta(\infty) = \frac{C - C_\infty}{C_w - C_\infty} \Rightarrow \theta(\infty) = \frac{C_\infty - C_\infty}{C_w - C_\infty} = 0, \tag{4.6.8}$$

the boundary conditions can be transformed as;

$$f(\eta) = 0,\ f'(\eta) = 1,\ \theta(\eta) = 1,\ \phi(\eta) = 1\ at\ \eta = 0. \tag{4.6.9}$$

$$f'(\eta) \longrightarrow \lambda,\ \theta(\eta) \longrightarrow 0,\ \phi(\eta) \longrightarrow 0\ as\ \eta \longrightarrow \infty. \tag{4.6.10}$$

4.7 Resulting equations after the similarity transformation

Through the use of suitable similarity transformation, the governing equations (3.6.1 - 3.6.4) and boundary conditions (3.6.5) and reduced to strongly nonlinear couple ODEs are then substituted in the (3.6.1 - 3.6.4) governing equations, and Ferdows *et al.* [16] use the following dimensionless variables.

$$\eta = y\sqrt{\frac{a}{\nu}},\ \psi = x\sqrt{a\nu}f(\eta),\ \theta(\eta) = \frac{T - T_\infty}{T_w - T_\infty},\ \phi(\eta) = \frac{C - C_\infty}{C_w - C_\infty}, \tag{4.7.1}$$

$\psi(x, y)$ is the stream function, η is the similarity variable, a is the intensity of the stagnation point in the above comparison. The stream function is satisfied by the continuity equation (3.6.1), which is written as;

$$u = \frac{\partial \psi}{\partial y} \text{ and } \nu = -\frac{\partial \psi}{\partial x}. \tag{4.7.2}$$

Using the equation (4.7.1) dimensionless variable, we get the following transformation of highly nonlinear coupled ODEs:

$$f''' + ff'' - (f')^2 + M\,(\lambda - f') + \lambda^2 + Gr\theta + Gc\phi = 0. \tag{4.7.3}$$

$$(1 + R)\theta'' + Ec\,Pr(f'')^2 + Pr\,f\theta' - m\,Pr\,f'\theta$$

$$+Pr\,Nb\phi'\theta' + Pr\,Nt(\theta')^2 + Pr\,S\theta = 0. \tag{4.7.4}$$

$$\phi'' + Le\,f\phi' + \frac{Nt}{Nb}\theta'' - \gamma Re_x Le\phi - m\,L\,f'\phi = 0. \tag{4.7.5}$$

Where $M = \frac{\sigma B_o^2}{\rho a}$ is magnetic parameter, $R = \frac{16\sigma T_\infty^3}{3k\,k^*}$ is a radiation parameter, $Ec = \frac{u_w^2}{c_p(T_w - T_\infty)}$ is Eckert number parameter, $G_r = g\frac{\beta_t(T_w - T_\infty)}{U}$ is the Grashoff number, $Gc = G\frac{\beta_t(C_w - C_\infty)}{U}$ modified Grashoff number, $Le = \frac{v}{D_B}$ is Lewis number parameter, $Pr = \frac{v}{\alpha}$ is the Prandtl number parameter, $\gamma = \frac{v\,K_o}{U^2}$ is chemical reaction parameter, $Re = \frac{x\,u_{w(x)}}{v}$ is the local Reynolds number, $Nb = \frac{(\rho c)_p D_B(\varphi_w - \varphi_\infty)}{v(\rho c)_f}$ is Brownian motion parameter, $S = \frac{Q}{\rho\,c_\rho\,a}$ is the heat generation/sink parameter, $Nt = \frac{(\rho c)_p D_B(T_w - T_\infty)}{v\,T_\infty(\rho c)_f}$ is thermophoresis parameter, constant parameter m and stretching parameter $\lambda = b/a$.

4.8 The quantities of physical interest

The physical quantities are reduced to Nusselt number (Nu), Sherwood number (Sh) and local skin friction coefficient are as follows:

$$C_f Re^{\frac{-1}{2}} = \left(\frac{xu_w}{v}\right)^{\frac{-1}{2}} \frac{\tau_w}{\left(\frac{\rho U^2}{2}\right)} = -f''(0), \tag{4.8.1}$$

where $Re_x = \frac{xu_w}{v}$ is the local Reynolds number and reduced local skin friction $f''(0)$. Then

$$NuRe^{\frac{-1}{2}} = \left(\frac{xq_w''}{D_B(\phi_w - \phi_\infty)}\right)\left(\frac{xu_w}{v}\right)^{\frac{-1}{2}} = -(1 + R)\theta'(0), \tag{4.8.2}$$

and,

$$ShRe^{\frac{-1}{2}} = \left(\frac{xq''_m}{D_B(\phi_w - \phi_\infty}\right)\left(\frac{xu_w}{v}\right)^{\frac{-1}{2}} \phi'(0) = -\phi'(0), \tag{4.8.3}$$

The velocity of the plate is denoted by U, reduced Nusselt number $\theta'(0)$ and reduced local Sherwood number $\phi'(0)$, q''_w and q''_m are the heat and mass flux, τ_w is the wall shear stress,ρ is the density of the fluid, u_w and u_m the stretching velocity m/s^{-1}.

Chapter 5

Numerical Solution Methods

This study considers the SLLM and SRM methods, which are based on the spectral process. Motsa [35] invented and popularized the SLLM and SRM techniques. Both SLLM and SRM are highly accurate algorithms with a wide convergence area. We solve the nonlinear ODEs using SLLM and SRM methods. We compare the results obtained from two numerical methods with those obtained from the bvp4c solver of the implicit Runge Kutta fourth order method.

5.1 Basic idea of the SLLM

We consider a system of differential equations let m be the number of differential equations, we have $z = [z_1(\eta), z_2(\eta), ..., z_m(\eta)]$ satisfies the system,

$$L_i[z_1(\eta), z_2(\eta), ..., z_m] + N_i[z_1(\eta), z_2(\eta), ..., z_m] = H_i(\eta),\ \ \eta\ \varepsilon\ [a, b], \tag{5.1.1}$$

where $i = 1, 2.., m$ and each H_i is a function of η, also linear L_i and nonlinear N_i components of differential equations, respectively. Basically the SLLM is an iterative method for solving differential equations such as equation (4.7.1) which start with an initial approximations z_i successive application of the SLLM.

$$z_r = [z_{1,r}(\eta), z_{2,r}(\eta), ..., z_{m,r}(\eta)] \text{ for each } r = 0, 1, 2..., \tag{5.1.2}$$

after the linearization of component of N_i, the differential equation (5.1.1) can be solved numerically using a Chebyshev spectral collocation method (5.1.2) which denote the i-th differential equation (5.1.3) after the first $(r + 1)$ iterations of the SLLM.

$$L_i\ |_{r+1} + N_i\ |_{r+1} = H_i. \tag{5.1.3}$$

The nonlinear component N_i can be linearized using the Taylor series,let w_r be an n-tuple of $Z_{i,r}$ and its derivative. If we assume that N_i is a function of w_r only, then linearization of N_i at W_r

$$N_i\ |_{r+1} = N_i\ |_r + \nabla N_i\ |_r\ (W_{r+1} - W_r), \tag{5.1.4}$$

where W_r is an n-tuple of $z_{i,r}$ and its derivatives (4.2.3) can be approximated as,

$$L_i \mid_{r+1} + \nabla N_i \mid_{r+1} * W_{r+1} = H_i + \nabla N_i \mid_r * W_r - N_i \mid_r, \tag{5.1.5}$$

equation (4.2.5) is then solved with Chebyshev spectral collocation method by Trefethen [50].

5.2 Application of SLLM

We solve the model equations (4.7.2 - 4.7.4) as follows:

$$f'_{r+1} = g_r, \tag{5.2.1}$$

$$g''_{r+1} + f_r g'_{r+1} + M\, g_{r+1} + 2 g_r g_{r+1} = -M\lambda - \lambda^2 + (g_r)^2 - Gr\theta - Gc\phi_r \tag{5.2.2}$$

$$(1+R)\theta''_{r+1} + Pr\, f_r \theta'_{r+1} - m\, Pr\, g_r \theta_{r+1} + Pr\, Nb \phi'_r \theta'_{r+1} + 2Pr\, Nt \theta'_r \theta_{r+1} + Pr\, S\theta_{r+1}$$

$$= Pr\, Nt (\theta'_r)^2 - Ec\, Pr\, (f''_r)^2. \tag{5.2.3}$$

$$\phi''_{r+1} + Le\, f_r \phi'_{r+1} - \gamma Re_x Le \phi_{r+1} - m\, Le g_r \phi_{r+1} = -\frac{Nb}{Nt}\theta''_r. \tag{5.2.4}$$

The boundary conditions are

$$f_{r+1}(\eta) = 0,\ g_{r+1}(\eta) = 1,\ \theta_{r+1}(\eta) = 1,\ \phi_{r+1}(\eta) = 1 \text{ at } y = 0. \tag{5.2.5}$$

$$g_{r+1}(\eta) \longrightarrow \lambda,\ \theta_{r+1}(\eta) \longrightarrow 0,\ \phi(\eta)_{r+1} \longrightarrow 0 \ as\ y \longrightarrow \infty. \tag{5.2.6}$$

Applying Chebyshev differentiation to equations (5..2.1 - 5.2.3), we get :

$$A_1 = D^2 + \text{diag}\{f_r\} D - 2\,\text{diag}\{g_r\} - M\, I \tag{5.2.7}$$

$$B_1 = -M\lambda - \lambda^2 - (g_r)^2 - Gr\theta - Gc\phi_r \tag{5.2.8}$$

$$A_2 = (1+R)D^2 + Pr\,\text{diag}\{f_r + Nb\phi'_r\} D + 2Pr\, Nt\,\text{diag}\{\theta'_r\} D$$

$$-m\, Pr\,\text{diag}\{g_r\} + Pr\, S\, I \tag{5.2.9}$$

$$B_2 = -Ec\,Pr g_r'^2 + Pr\,Nt(\theta_r')^2 \tag{5.2.10}$$

$$A_3 = D^2 + Le\,\mathrm{diag}\{f_r\}D - Le\,m\,\mathrm{diag}\{g_r\} - Le\gamma Re\,I \tag{5.2.11}$$

$$B_3 = \frac{Nt}{Nb}\Theta_r'' \tag{5.2.12}$$

where diag represents a diagonal matrix. The equations (4.7.6 - 4.7.7) satisfies the boundary conditions for an identity matrix (I) of size $(\bar{N}+1)\times(\bar{N}+1)$ where $(\bar{N}+1)$ is the number of collocation points. For equations (4.7.2 - 4.7.4), the initial guess for the SLLM scheme are functions that satisfy the boundary conditions. The temperature, velocity and concentration profiles for the boundary layer problem are discussed in this study based on a physical understanding of how they decay exponentially as $\eta \to \infty$. The initial guesses are chosen in the following order to fulfill the boundary conditions (5.2.10 - 5.2.11):

$$f_0(\eta) = 1 - e^{-\eta},\ \theta_0(\eta) = e^{-\eta},\ \phi_0(\eta) = e^{-\eta}. \tag{5.2.13}$$

The iterative procedure is stopped after the corresponding solutions f_{r+1}, θ_{r+1}, ϕ_{r+1} for each $r > 1$ satisfy the convergence tolerance of $\varepsilon = 10^{-8}$. That is iterative procedure is stopped when $E_d = max(||f_{r+1} - f_r||_\infty, ||\theta_{r+1} - \theta_r||_\infty, ||\phi_{r+1} - \phi_r||_\infty,) < \varepsilon$ where E_d is difference error.

5.3 Basic idea of the SRM

We give a brief description of the SRM which can be applied to equations (4.7.2 - 4.7.4). Like SLLM, the SRM also imports the Gauss Seidel idea for decoupling the system into sequence of subsystem. The iteration method of the solution is developed through the application of simple iteration method (SIM) so that we can apply SRM as follows: Consider n-th order nonlinear differential equation expressed in terms of the nonlinear operation F as

$$F[y(x), y'(x), ..., y^{(n)}(x)] = 0. \tag{5.3.1}$$

To develop the iteration scheme of equation (5.3.1) is expressed as a sum of its linear and nonlinear components as

$$F[y, y', ..., y^{(n)}] = L[y, y', ..., y^{(n)}] + N[y, y', ..., y^{(n)}] = 0, \tag{5.3.2}$$

through minimizing of the equation (5.3.2), can be written as

$$F[y^{(i)}]_{i=0}^{n} = L[y, y', ..., y^{(n)}] + N[y, y', ..., y^{(n)}] = 0, \tag{5.3.3}$$

where

$$[y^{(i)}]_{i=0}^{n} = [y^{(0)}(x), y^{(1)}(x), y^{(2)}(x), ..., y^{(n)}(x)], \tag{5.3.4}$$

for nonlinear component N is provided and be written as the sum of nonlinear terms,

$$N[y^{(k)}]_{k=0}^{n} = y^{(n)}N_n[y^{(k)}]_{k=0}^{n} + y^{(n-1)}N_{n-1}[y^{(k)}]_{k=0}^{n-1} + ... + y^{(2)}N_2[y^{(k)}]_{k=0}^{2}$$

$$+y^{(1)}N_1[y^{(k)}]_{k=0}^{1} + y^{(0)}N_0[y^{(k)}]_{k=0}^{0}. \tag{5.3.5}$$

The simple iteration method is developed for differential equation as follows:

$$\sum_{k=0}^{n} \alpha_k(x)y_{r+1}^{(k)} + \sum_{k=0}^{n} y_{r+1}^{(k)}N_k[y_r^{(i)}]_{i=0}^{k} = 0, \tag{5.3.6}$$

where

$$\sum_{k=0}^{n} \alpha_k(x)y_{r+1}^{k} = L[y_{r+1}^{(k)}]_{i=0}^{n}. \tag{5.3.7}$$

The subscript $r+1$ stands for the current iteration level. The equation (5.3.6) and initial guess $y_0(x)$ can be used to obtain successive approximations, $y_{r+1}(x)$, for differential equation (5.3.7) for r= 0, 1, 2..., the simple iteration scheme is linear can be solved, subject to appropriate boundary conditions. In terms of the spectral collocation method continuous derivatives are evaluate at the $M+1$ collocation point x_s for $s = 0, 1, ..., M$ to obtain the transformation

$$y^{(i)}(x_s)D^{(i)}Y. \tag{5.3.8}$$

Where D is the so called differention matrix and

$$Y = [y(x_0), y(x_1), ..., y(x_{m-1}), y(x_m)]^T. \tag{5.3.9}$$

applying equation (5.3.7) in the iteration scheme (5.3.6) gives

$$AY = B, \tag{5.3.10}$$

then

$$A = \sum_{i=0}^{n}[\alpha D^i + \beta], \beta_k = N_k[y_r^{(i)}]_{i=0}^{k}, \tag{5.3.11}$$

where B is a vector with elements taken from the problem's boundary condition, α and β are diagonal matrices obtained from evaluating α and β at the collocation point. The coupled equations (4.7.2 - 4.7.4) can be configured to a form convenient direct application of the SIM scheme and also tested SRM on the well-known boundary layer problem. The vector is defined by z_i and derivatives of the variable z_i with respect to η, so

$$z_i(\eta) = [z_i^{(0)}, z_i^{(1)}, ..., z_i^{(n_i)}]. \tag{5.3.12}$$

• The equation of the written in term of z_i and sum of its linear (L_i), and non-linear (N_i) components where;

$$L_i[z_1, z_2, z_3..., z_m] + N_i[z_1, z_2, z_3, ..., z_m] = H_i, i = 1, 2, 3, .., m \tag{5.3.13}$$

• The H_i is a known function of η by applying the SRM and implementing the boundary conditions.

5.4 Application of SRM

The SRM follows the same methodology as the SLLM. We write the iteration scheme as follows, using the equations (4.7.2 - 4.7.4).

$$f'_{r+1} = g_r. \tag{5.4.1}$$

$$g''_{r+1} + f_r g'_{r+1} - g_r^2 + M\lambda - g_{r+1} + \lambda^2 + Gr\theta + Gc\phi_r = 0. \tag{5.4.2}$$

$$(1+R)\theta''_{r+1} + Ec\, g'^2_{r+1} + Pr\, f_r\theta'_{r+1} - m\, Pr\, g_{r+1}\theta_{r+1} + Pr\, Nb\phi'_r\theta'_{r+1}$$

$$+PrNt(\theta'_r)^2 \pm Pr\, S\theta_{r+1} = 0. \tag{5.4.3}$$

$$\phi''_{r+1} + Le\, f_r\phi'_{r+1} + \frac{Nt}{Nb}\theta''_r - \gamma Re_x Le\phi_{r+1} - m\, Leg_{r+1}\phi_{r+1} = 0. \tag{5.4.4}$$

The boundary conditions become:

$$f_{r+1}(\eta) = 0,\ g_{r+1}(\eta) = 1,\ \theta_{r+1}(\eta) = 1,\ \phi_{r+1}(\eta) = 1 \text{ at } y = 0. \tag{5.4.5}$$

$$g_{r+1}(\eta) \longrightarrow \lambda,\ \theta_{r+1}(\eta) \longrightarrow 0,\ \phi(\eta)_{r+1} \longrightarrow 0 \text{ as } y \longrightarrow \infty. \tag{5.4.6}$$

as in SLLM, applying the Chebyshev differentiation and using similar approach for the SRM gives the following:

$$A_1 = D^2 + \text{diag}\{f_r\}D - M\, I, \tag{5.4.7}$$

$$B_1 = -M\lambda - \lambda^2 + g_r^2 - Gr\theta - Gc\phi, \tag{5.4.8}$$

$$A_2 = (1+R)D^2 + Pr\,\text{diag}\{f_r + Nb\phi'_r\}D - m\, Pr\,\text{diag}\{g_r\} + Pr\, S\, I, \tag{5.4.9}$$

$$B_2 = -Ec\,Pr\,g_r'^2 - Pr\,Nt(\theta_r')^2, \tag{5.4.10}$$

$$A_3 = D^2 + Le\,\mathrm{diag}\{f_r\}D - m\,Le\,\mathrm{diag}\{g_r\} - \gamma Re_x Le\,I, \tag{5.4.11}$$

$$B_3 = -\frac{Nt}{Nb}\theta_r'', \tag{5.4.12}$$

The initial guesses for satisfying the boundary conditions (5.2.10 - 5.2.11):

$$f_0(\eta) = 1 - e^{-\eta},\ \theta_0(\eta) = e^{-\eta},\ \phi_0(\eta) = e^{-\eta}. \tag{5.4.13}$$

The iterative procedure is stopped after the corresponding solutions f_{r+1}, θ_{r+1}, ϕ_{r+1} for each $r > 1$ satisfy the convergence tolerance of $\varepsilon = 10^{-8}$. That is iterative procedure is stopped when $E_d = max(||f_{r+1} - f_r||_\infty, ||\theta_{r+1} - \theta_r||_\infty, ||\phi_{r+1} - \phi_r||_\infty,) < \varepsilon$ where E_d is difference error.

5.5 Test for convergence

This summary on how to test for convergence is derived from Mdziniso [31]. We evaluate the error due to decoupling (E_d) of the unknown functions at each $(r+1)^{th}$ iteration.

$$E_d = \max(\|n_{i,r+1} - n_{1,r}\|_\infty, \|n_{2,r+1} - n_{2,r}\|_\infty, ...\|n_{m,r+1} - n_{m,r}\|_\infty). \tag{5.5.1}$$

Where $n_i, i = 1, 2, 3, ..., m$ are the controlling unknown functions. We consider the error caused by decoupling at each r^{th} iterative step, given by e_r, where $r = 1, 2, 3..., M$, where M is the total number of iterations. Because two iterations, (E_d) is essentially the infinity norm of the solutions to each unknown. The convergence occurs if,

$$e_1 < e_2 < e_3 < .... < e_M. \tag{5.5.2}$$

Basically the iterative scheme is convergent if and only if (E_d) is inversely proportional to the number of iterations. The convergence tolerance is considered to be $\varepsilon = 10^{-8}$ in this study, and the iterative procedure is terminated when the following condition is met,

$$\frac{\|X_{r+1} - X_r\|_\infty}{\|X_{r+1}\|_\infty} \leq \varepsilon, \tag{5.5.3}$$

where ε is the convergence tolerance level and X_r represent it is unknown function at iteration r. The effect of the number of collocation point N was observed in order to select the smallest value of$N$ which gives a steady solution to the ε error level. To upgrade the convergence rate

we apply the spectral relaxation method SRM. The SRM scheme for solving the function say X at the $(r+1)^{th}$ iteration give as follows:

$$AX_{r+1} = B, \tag{5.5.4}$$

then upgrade version of the SRM is

$$AX_{r+1} = (1-w)AX_r + wB, \tag{5.5.5}$$

where A and B are matrices and w is the convergence controlling relaxation parameter. Then when $w = 1$ is substituted in equation (5.5.4) reduces the original SRM method. Figure 5.1 show the demonstrate of the convergence and stability of the SLLM. The SRM log-eror plot for the problem steady MHD boundary layer flow and heat transfer characteristics are given in is clear that the logarithm of the number of iteration when heat source parameter is varied. The governing values of the unsteady or steady parameters used are: $Pr = 10$, $Nt = 0.1$, $Gr = 7$, $Gc = 0.5$, $\lambda = 0$, Nb=0.1, Re=1, Ec=0.1, m=1, R=1 and $\gamma = 0.1$. During the computation by each iterative technique, the tolerance was specified to be (Ed) less than 10^{-8}. We can observe that the SLLM technique ensures a maximum number of iterations, so that as the number of iterations increases, Ed decreases as they converge to the inaccurate answer.

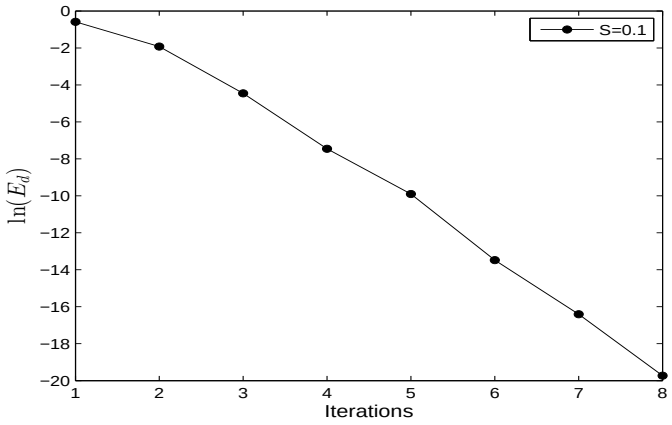

Figure 5.1: Logarithm of SRM decoupling error

Chapter 6

Results and Discussion

The numerical study of steady MHD boundary layer flow over a stretching sheet in the presence of heat generation/absorption and nanofluid chemical reaction has been investigated. The spectral relaxation method (SRM) is used to solve the transformed nonlinear ordinary differential equations (4.7.2 - 4.7.4), with the boundary conditions (4.7.5 - 4.7.6), and the results are compared to the spectral local linearization method (SLLM).

The values of the unsteady or steady parameters are as follows: $Pr = 10$, $Nt = 0.1$, $Gr = 7$, $Gc = 0.5$, $\lambda = 0$, Nb=0.1, Re=1, Ec=0.1, m=1, R=1, $\gamma = 0.1$ and S=0.1 Ferdows *et al.* [16]. The effects of physical parameters on dimensionless velocity, temperature, and concentration are investigated, as well as the local skin friction coefficient, local Nusselt number, and local Sherwood number. In all cases, the number collocation points of both SRM and SLLM were $N_x = 100$ and a finite computational value of $\eta_\infty = 30$ was chosen in the η direction. The tolerance level for each method was set to $\varepsilon = 10^{-8}$. To verify the accuracy and validate the SRM and SLLM, the results are presented and compared with the bvp4c solver of implicitly Runge-Kutta fourth order process in terms of the number of iteration step (iter) and the computing times. The Matlab programming language was used on the windows 10 platform AMD E2-7119 APU with AMD Radeon R2 Graphic 1.80 GHZ. 4.00 GB speed ADM.

Table 6.1: Comparison of the SRM, SLLM and those obtained by bvp4c of current results for $f''(0)$ when varying stretching parameter (λ)

			SRM			*SLLM*			*bvp4c*
λ	iter	time(sec)	$f''(0)$	iter	time(sec)	$f''(0)$	iter	time(sec)	$f''(0)$
0.1	26	36.519939	1.72998286	09	8.235677	1.72998286	30	189.8765	1.72998286
0.3	29	20.968766	0.77085842	08	10.875781	0.77085842	34	289.603919	0.77085842
0.4	54	31.136881	0.87180975	09	7.942629	0.87180975	37	366.604432	0.87180975

Table 6.1 shows a comparison of SLLM and SRM results to the bvp4c result. Table 6.1 shows the effects of increasing the stretching parameter λ on the reduced local skin coefficient $f''(0)$. The output of two methods and also the bvp4c method were compared by

testing computational time required to generate the results. We can see that the SLLM takes less time to compute than SRM and bvp4c, and that bvp4c is the slowest to converge. The results of the SRM, SLLM, and bvp4c methods all have the same $-f''(0)$ values. Table 6.1 shows that SLLM is the better method because it is faster than SRM and bvp4c. As a result, the rest of the results will be produced by SLLM and shown in tabular and graphic form.

Table 6.2: Comparison of SLLM and SRM with different value of S and γ

			$\theta'(0)$	$\phi'(0)$			$\theta'(0)$	$\phi'(0)$
γ	$iter$	$time(tsec)$	SRM	SRM	$iter$	$time(sec)$	$SLLM$	$SLLM$
0.08	27	23.149603	1.72748747	3.59419487	07	6.763667	1.72748747	3.59419487
0.1	26	36.519939	1.72998286	3.54856202	09	8.235677	1.72998286	3.54856202
0.3	12	26.604175	1.73167707	3.84273570	09	19.021493	1.71429634	3.84273570
S								
0.04	25	26.808476	1.77900595	3.51389970	07	19.236405	1.77900595	3.51389970
0.06	12	6.440782	1.76276680	3.52540393	09	6.894574	1.76276680	3.52540393
0.1	26	36.519939	1.72998286	3.54856202	09	8.235677	1.72998286	3.54856202

Table 6.2 compares the two approaches used for different chemical reaction (γ) and heat source/sink parameter (S) on reduced Nusselt number $\theta'(0)$ and reduced local Sherwood number $\phi'(0)$. When comparing the numerical results obtained, it is clear that the SLLM is the superior approach to the SRM in terms of the nuber of iterations and computing times.

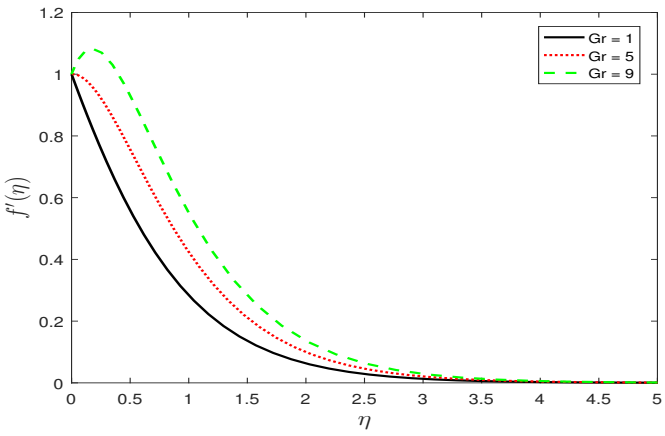

Figure 6.1: The effects of Grashof number (Gr) of the velocity profile

The effect of the thermal Grashof number (Gr) on the velocity profile is shown in Figure 6.1. We noticed that as the Grashof number (Gr) rises, so does the velocity profile. Since the Grashof number (Gr) is the ratio of buoyancy to viscous forces in the boundary layer, it induces an increase in buoyancy forces relative to viscous forces in the boundary layer, which influences the velocity in the field.

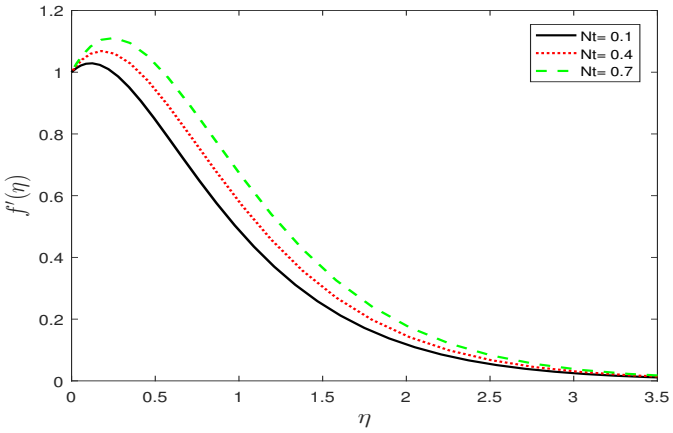

Figure 6.2: The effects of thermophoresis parameter (Nt) of the velocity profile

Figure 6.2 shows how the thermophoresis parameter (Nt) affects the velocity profile. We observe that the velocity profile increase with an increase of the (Nt).We observe that the velocity profile increases with an increase of (Nt). This is due to the fact that the thermophoresis parameter (Nt) is the transport force that arises as a result of the existence of a temperature gradient.

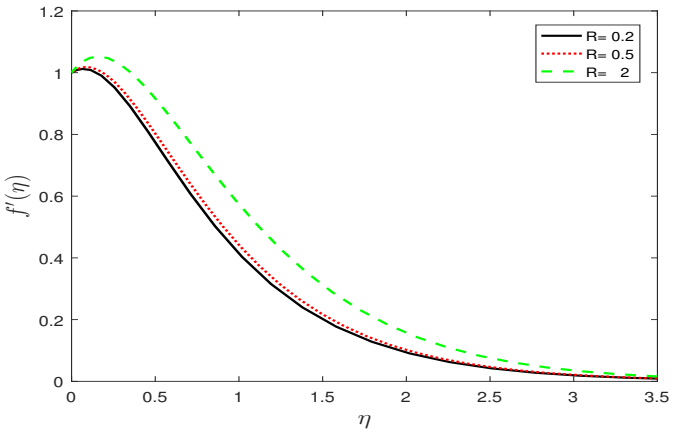

Figure 6.3: The effects of radiation parameter (R) of the velocity profile

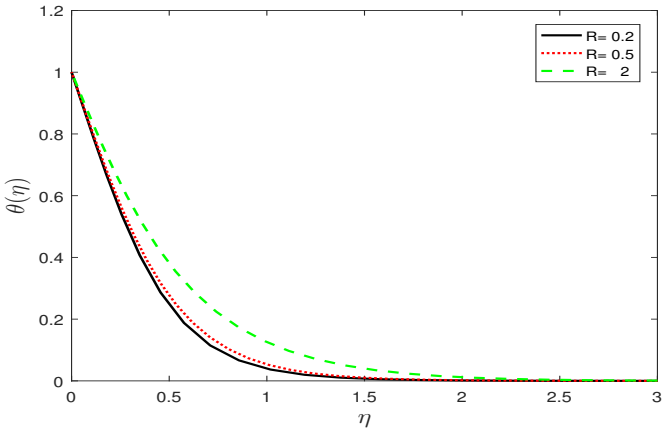

Figure 6.4: The influence of the radiation parameter (R) temperature profile

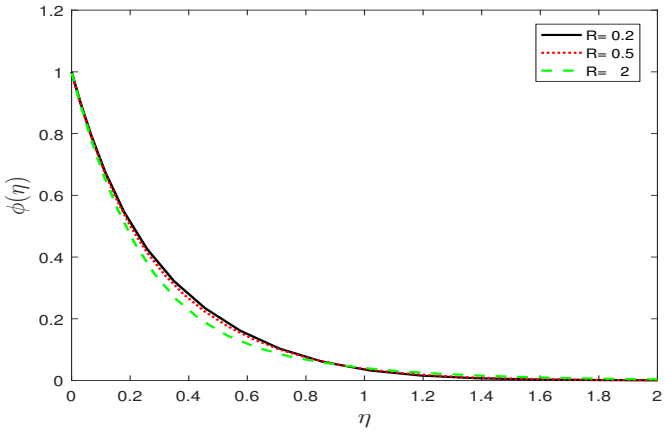

Figure 6.5: The influence of the radiation parameter (R) on the concentration profile

Figures 6.3, 6.4 and 6.5 display the influence of the radiation parameter (R) on the velocity, temperature and concentration profiles. As the value of the radiation parameter (R) rises, so does the velocity and temperature profile. The relative contribution of conduction heat transfer to thermal radiation transfer is defined as the radiation parameter (R). As the radiation parameter (R) increases, the temperature inside the boundary layer rises, causing the velocity to rise. As a result, the decrease in the concentration profile is influenced.

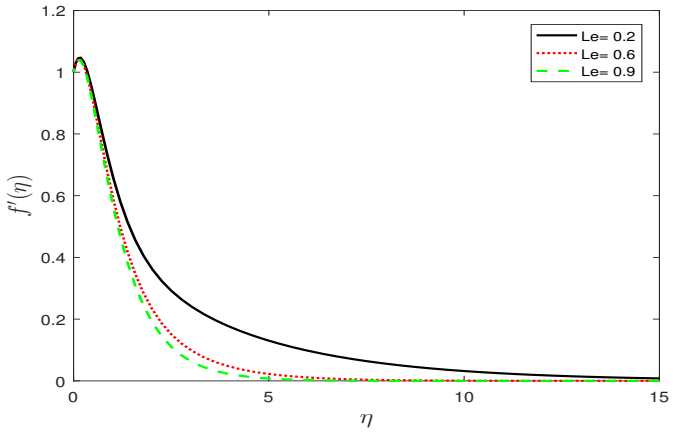

Figure 6.6: The effects of the Lewis number (Le) of the velocity profile

Figure 6.6 shows the effect of Lewis number (Le) velocity profile. It can be seen that as Lewis number (Le) increases when the velocity decreases. The heat transfer rate falls while the mass transfer rate increases.

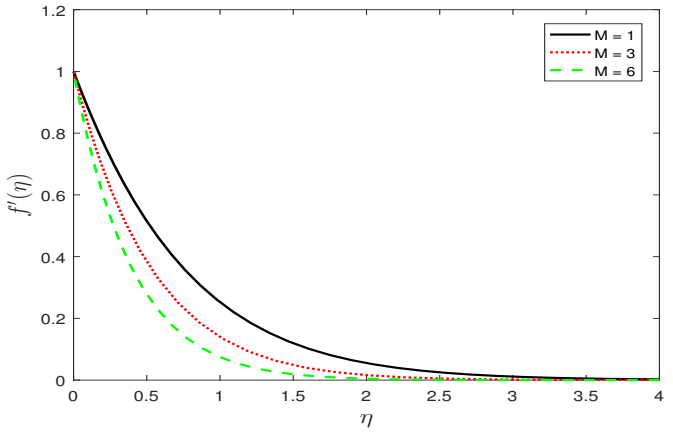

Figure 6.7: The effects magnetic parameter (M) on the velocity profile

The effect of magnetic parameter (M) on the velocity profile is shown in Figure 6.7. Since the Lorentz force is generated by applying a magnetic field to an electrically conducting fluid, the velocity profile decreases as the magnetic parameter (M) increases, thickening the boundary layer. The force is similar to a drag force, causing the velocity to decrease.

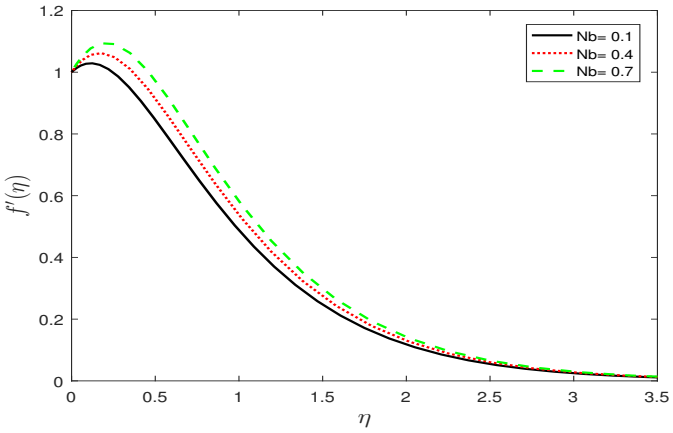

Figure 6.8: The effects of the Brownian motion (Nb) on the velocity profile

Figure 6.8 depicts the effects of Brownian motion (Nb) on the velocity profile. As the Brownian motion (Nb) increases, so does the velocity profile. In all liquids and gases, particles travel at random, causing larger particles to be carried by light fast moving molecules.

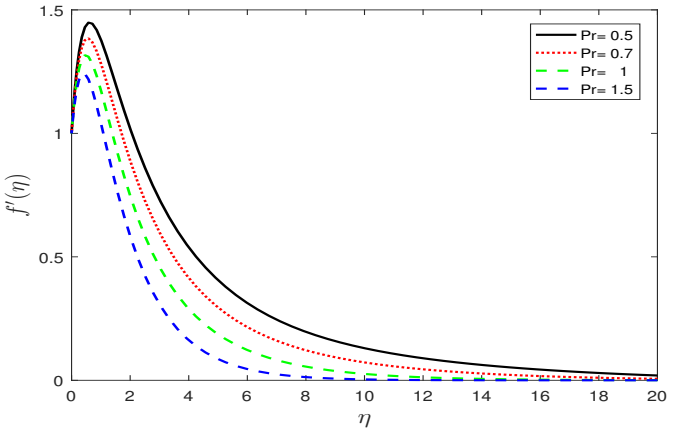

Figure 6.9: The effects of the Pandtl number (Pr) on the velocity profile

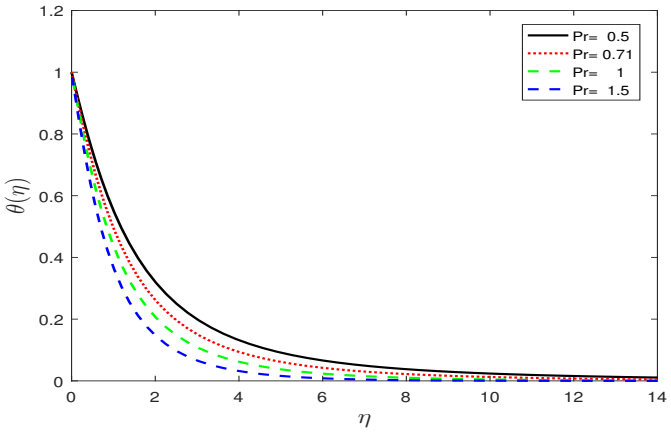

Figure 6.10: The influence of the Pandtl number (Pr) on the temperature profile

Figures 6.9 and 6.10 show the effects of the Pandtl number (Pr) on velocity and temperature profiles. It can also be seen that increasing the Prandtl number Pr the temperature of the fluid because of the decrease of the thermal boundary layer thickness.

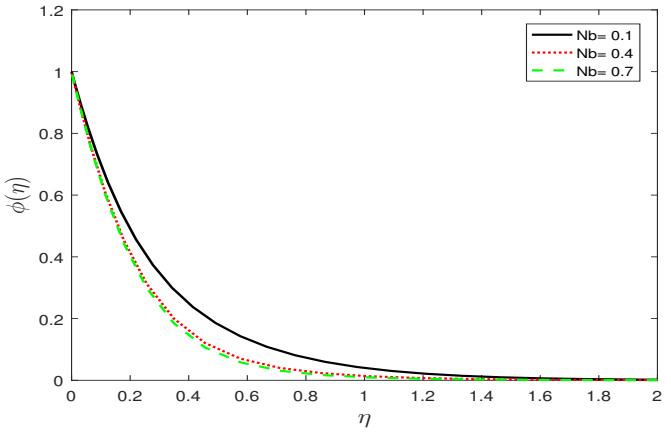

Figure 6.11: The influence of the Brownian motion (Nb) on the concentration profile

The effect of the Brownian motion parameter (Nb) on the dimensionless concentration $\phi(\eta)$ profile is shown in Figure 6.11. It is found that larger Brownian motion parameter (Nb), results in a poor reduction in dimensionless species concentration profile. The argument for this is that as Brownian motion increases, so does random motion and collision of the fluid's nanoparticles, lowering the fluid's concentration.

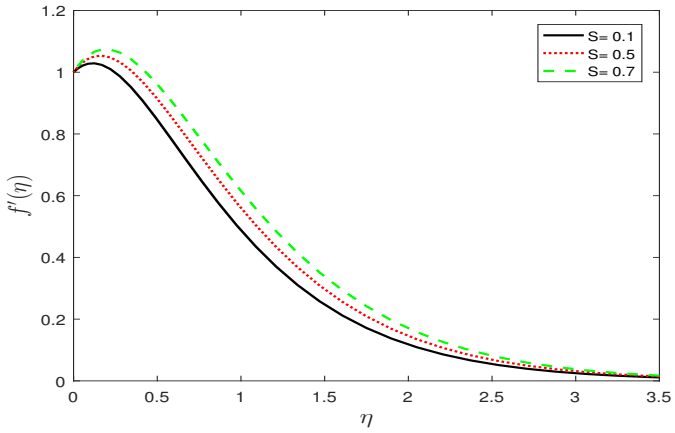

Figure 6.12: The effects of the heat source/sink parameter(S) on the velocity profile

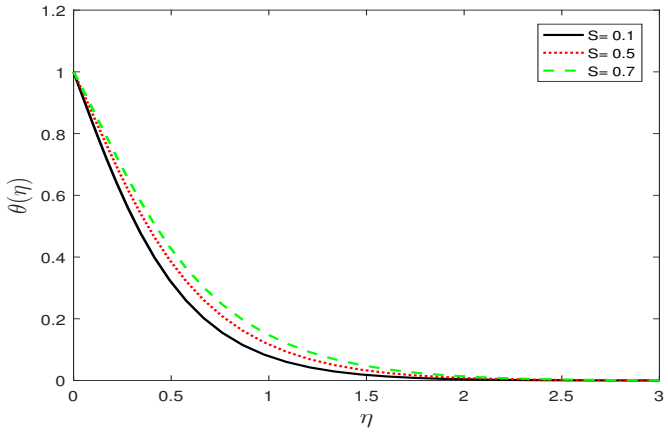

Figure 6.13: The influence of the heat source/sink parameter (S) on the temperature profile

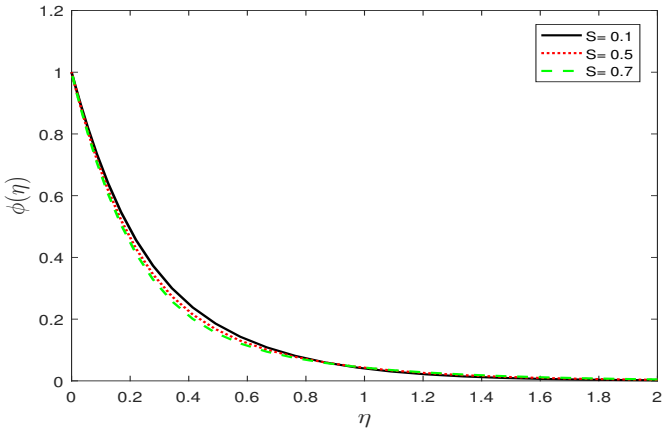

Figure 6.14: The influence of the heat source/sink parameter (S) on the concentration profile

The effect of the heat source/sink parameter (S) is shown in Figures 6.12, 6.13 and 6.14 where an increase in the heat source/sink parameter (S) results in an increase in velocity and temperature, but a decrease in concentration. The concentration species were reduced due to the heat source/sink parameter (S) because heat generation increases the momentum and thermal boundary layer thickness while decreasing the nanofluid concentration boundary layer thickness.

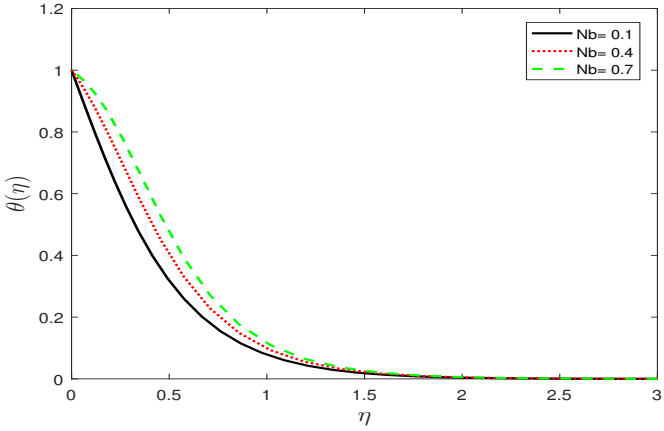

Figure 6.15: The influence of the Brownian motion (Nb) on the temperature profile

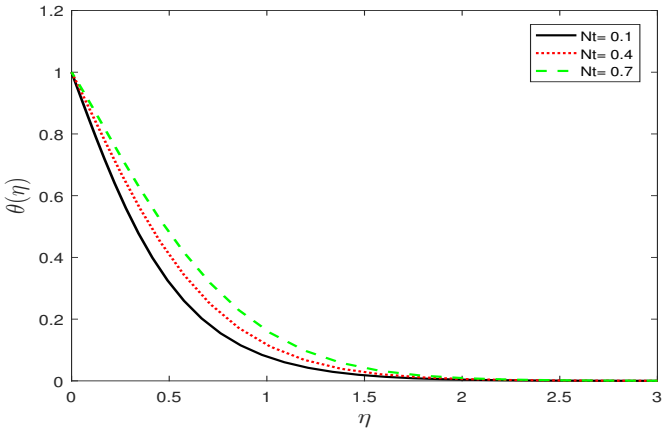

Figure 6.16: The influence of the thermophesis parameter (Nt) on the temperature profile

The effect of the Brownian motion parameter (Nb) and the thermophoresis parameter (Nt) on the dimensionless temperature $\theta(\eta)$ profile is shown in Figures 6.15 and 6.16. As the value of the Brownian motion parameter (Nb) increases in Figure 6.15 , the temperature rises, Brownian motion is responsible for a nanofluid's thermal conductivity. However, as Brownian motion parameter Nb levels increase and we can see that the thermophoresis parameter (Nt) increase as the temperature approaches the wall.

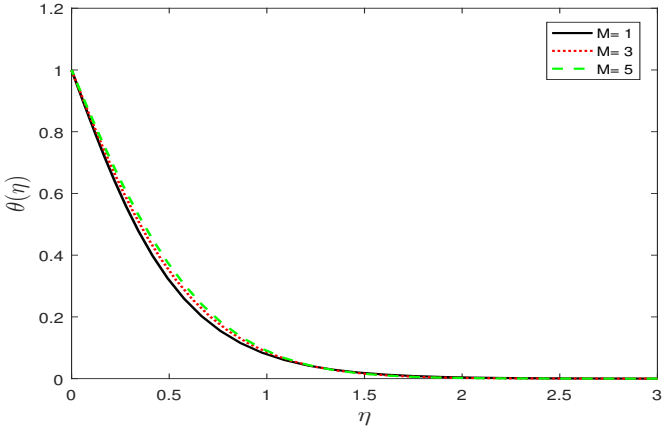

Figure 6.17: The influence of the magnetic parameter (M) on the temperature profile

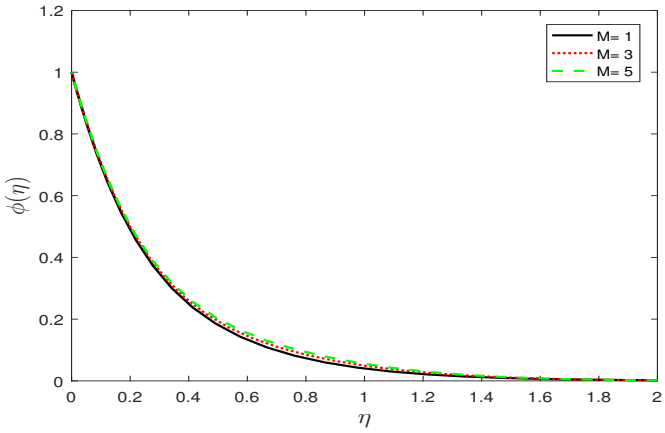

Figure 6.18: The influence of the magnetic parameter (M) on the concentration profile

In Figures 6.17 and 6.18, we display the effect of magnetic field parameter (M) on the dimensionless temperature $\theta(\eta)$ and dimensionless concentration $\phi(\eta)$ distribution profile respectively. It is observed that steady increasing both temperature $\theta(\eta)$ and concentration $\phi(\eta)$ when the magnetic field parameter (M) increases. This is because when a transverse magnetic field is applied to an electrically conducting fluid, it causes the Lorentz force, which is a resistive force. This force causes resistance in the fluid by increasing friction between its layers, resulting in an increase in temperature and concentration.

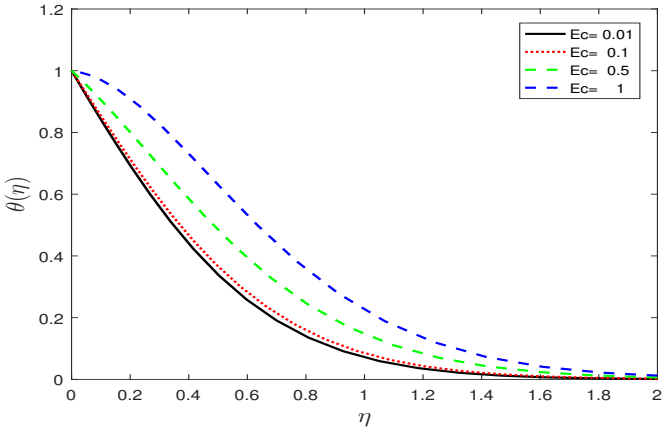

Figure 6.19: The influence of the Eckert number(Ec) temperature profile

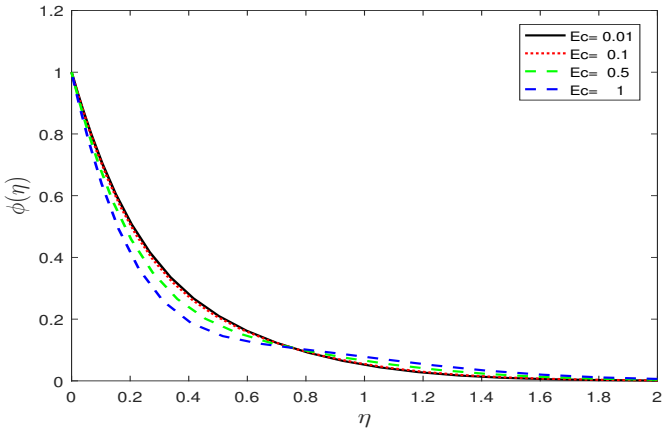

Figure 6.20: The influence of the Eckert number(Ec) on the concentration profile

We show the effect of Eckert number (Ec) on the dimensionless temperature $\theta(\eta)$ and dimensionless concentration $\phi(\eta)$ distributions in Figures 6.19 and 6.20, respectively. Eckert number (Ec) increases as temperature drops and concentration profile rises. The Eckert number (Ec) is the ratio of the flow's kinetic energy to the enthalpy difference between the boundary layers. This is because viscous dissipation generates heat as a result of drag between nanofluid particles, and this extra heat causes the initial fluid temperature to rise. The existence of viscous dissipation causes the momentum and heat boundary layers to thicken while the concentration boundary layer's thickness decreases.

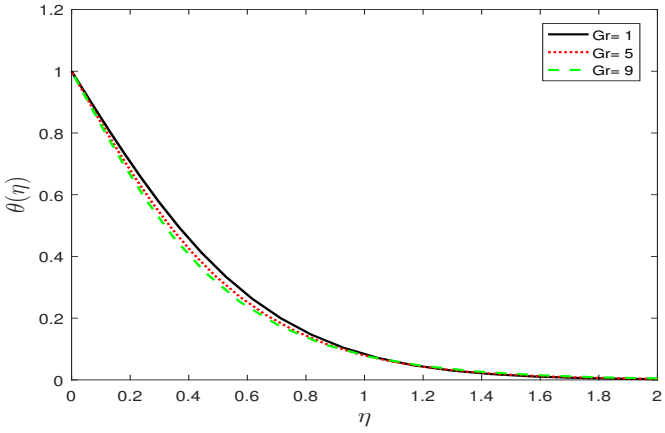

Figure 6.21: The influence of the Grashof number (Gr) on the temperature profile

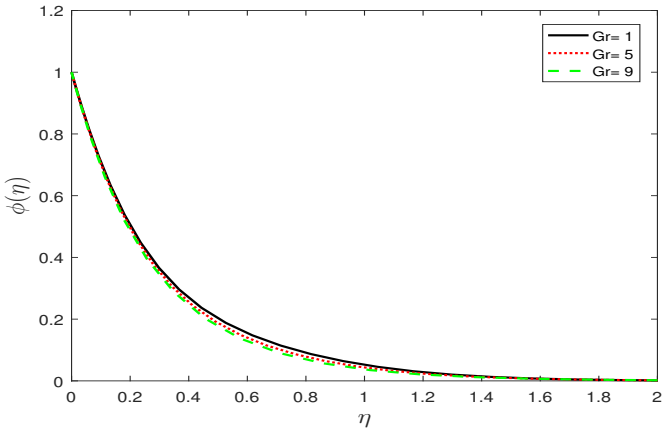

Figure 6.22: the influence of the Grashof number (Gr) on the concentration profile

The effect of Grashof number (Gr) on temperature and concentration profile are represented in Figures 6.21 and 6.22. We notice that the temperature and concentration profiles decrease with the increase on Grashof number (Gr). As the Grashof number (Gr) rises, the thermal boundary layer and the concentration boundary layer both shrink, lowering the fluid temperature everywhere but not next the wall.

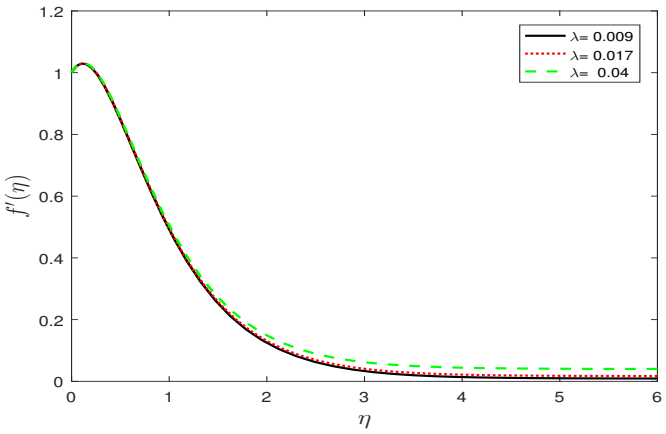

Figure 6.23: The effects of the stretching parameter (λ) on the velocity profile

Figure 6.23 depicts the effect of stretching parameter(λ) in velocity profile. It is noticed that the velocity profile increase as the stretching parameter (λ) increase. This is because the sheet after being stretched is now smoother and the fluid flow is faster than stretching sheet.

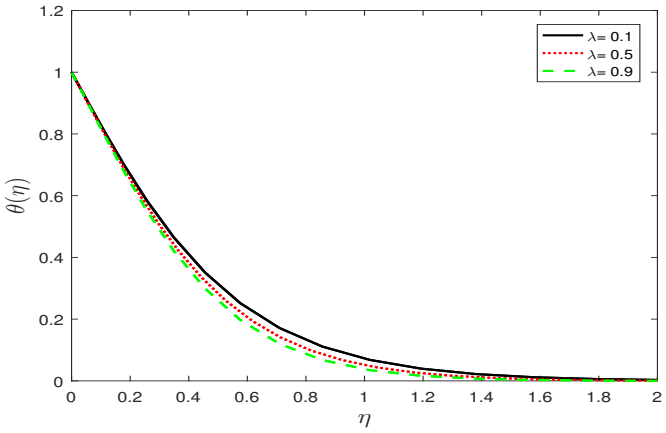

Figure 6.24: The influence of the stretching parameter (λ) on the temperature profile

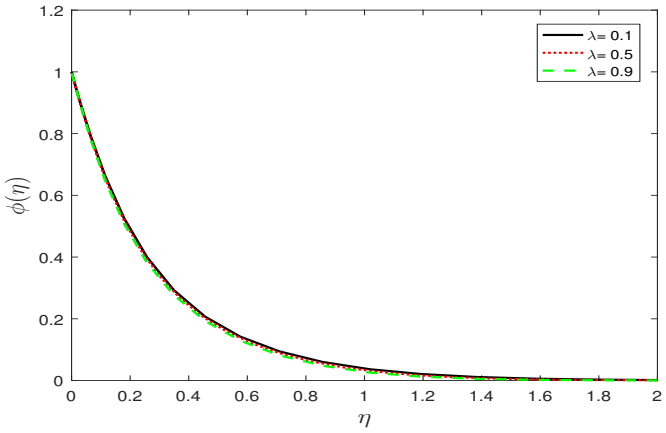

Figure 6.25: The influence of the stretching parameter (λ) on the concentration profile

In Figures 6.24 and 6.25, we show dimensionless temperature $\theta(\eta)$ and dimensionless concentration $\phi(\eta)$. Since the stretching parameter (λ) is a criteria relative effect of momentum, energy and mass diffusion equation in temperature and concentration respectively. It is seen that an increase in stretching parameter (λ) causes a decrease in both temperature and concentration profile.

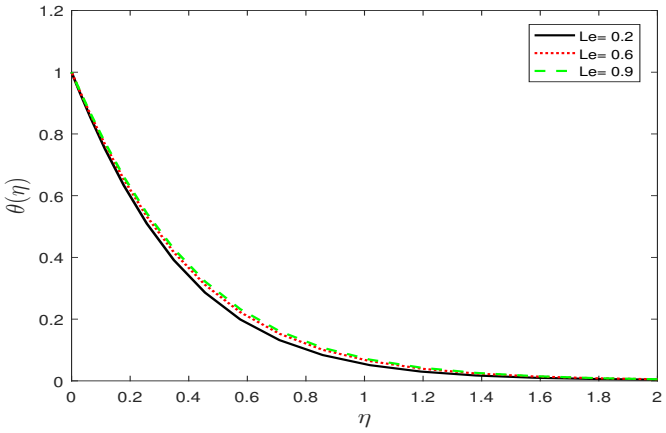

Figure 6.26: The influence of the Lewis number (Le) on the temperature profile

Figure 6.26 represents the effect of Lewis number (Le) on the dimensionless $\theta(\eta)$ distribution profile. It is observed that the temperature increase with the increase of Lewis number (Le). The nanoparticle volume percentage and nanoparticle volume boundary layer thickness both decrease dramatically when the Lewis number (Le) rises.

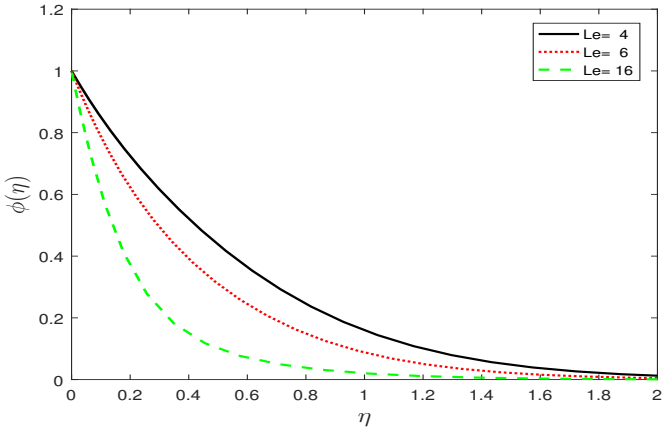

Figure 6.27: The influence of the Lewis number (Le) on the concentration profile

This Figure 6.27 show dimensionless velocity $f'(\eta)$ and dimensionless concentration $\phi(\eta)$ at a point of flow decreases toward the wall with an increase in the Lewis number Le.. In the boundary layer regime, the Lewis number is the ratio of thermal diffusion rate to species diffusion rate. The concentration profile will be suppressed if the Lewis number is increased.

Chapter 7

Conclusion and Recommendation

7.1 Conclusion

The effect of heat generation/absorption and chemical reaction on magnetohydrodynamics boundary layer flow of nanofluid over a stretching sheet was investigated in this study. Using similarity transformations, the governing nonlinear partial differential equation was transformed into nonlinear ordinary differential equations, which were then numerically solved using both the spectral local linearization method (SLLM) and the spectral relaxation method (SRM). The reduced local skin-friction $f'(\eta)$, the reduced Nusselt number $-\theta'(\eta)$ and the reduced Sherwood number $-\phi'(\eta)$ numerical results are presented in tabular form. For various governing parameters, the dimensionless velocity, temperature and concentration profile along the stretching sheet was investigated and the results were graphically displayed. To check the accuracy of SLLM and SRM they were compared to the Matlab bvp4c solver of the implicit Runge Kutta fourth order method. The following is the conclusion drawn from this study:

• The results of the SLLM process were similar to those of the SRM and bvp4c methods. The findings show that the three methods produce similar results. The results of the SRM, SLLM, and bvp4c methods all have the same reduced local skin coefficient $-f''(0)$ values. We infer from the results that heat generation/absorption and chemical reactions have an effect on velocity, temperature and concentration.

• We noticed that Grashof number (Gr) rises, so does the velocity profile. This shows that the heat transfer on the local skin coefficient transfers on the wall. Since Grashof number (Gr) is ratio of buoyancy to viscous forces in the boundary layer it causes an increase in the buoyancy forces relative to the viscous forces which influence the velocity in the boundary layer region.
• Thermophoresis parameter (Nt) increased because the transport force that occurs due to the presence of a temperature gradient hence as result of force the velocity increases. We observed that the increases of velocity profile increases the (Nt). This is due to the fact

that the thermophoresis parameter (Nt) is the transport force that arises as a result of the existence of a temperature gradient because as the force of the velocity increases so does the force of the velocity.

• An increase in the heat source parameter (S) results in an increase in velocity and temperature, but a decrease in concentration. The concentration diffusion species were reduced due to the heat source parameter (S). Heat generation increases the momentum and thermal boundary layer thickness while decreasing the nanofluid concentration boundary layer thickness.
• The thermophoresis and Brownian motion parameters dominated the heat transfer performance. Increasing Brownian motion and thermophoresis also increase temperature.
• It is observed that both temperature $\theta(\eta)$ and concentration $\phi(\eta)$ steadily increase when the magnetic field parameter (M) increases. This is because when a transverse magnetic field is applied to an electrically conducting fluid, it causes the Lorentz force which is a resistive force. This force causes resistance in the fluid by increasing friction between its layers resulting in an increases in temperature and concentration.
• It is noted that increasing temperature the compression Eckert number (Ec) increase because of the effect of dissipation due to internal friction of the fluid. The Eckert number (Ec) is the ratio of the flow's kinetic energy to the enthalpy difference between the boundary layers. This is because viscous dissipation generates heat as a result of drag between nanofluid particles, and this extra heat causes the initial fluid temperature to rise.
• It is seen that an increase in stretching parameter (λ) causes a decrease in both temperature and concentration profile. Because the momentum, energy, and mass diffusion are all connected in the current approach, this outcome is expected.

7.2 Recommendations

The influence of two-dimensional magnetohydrodynamics of a nanofluid over a stretching sheet in the presence of chemical reaction, heat generation, or absorption, buoyancy force thermal expansion and buoyancy force concentration expansion is presented in this thesis. Using a similarity transformation, the governing partial differential equations for momentum, energy, and concentration are determined and transformed to non-linear similar equations. The dimensionless nonlinear differential equations that result are numerically solved using the well-known spectral local linearization method (SLLM) and spectral relaxation method (SRM). Different parameters, such as Lewis number, Eckert number, modified Grashoff number, Grashoff number, stretching constant, chemical reaction, local Reynolds number, Prandtl number, heat source/sink, Brownian motion, and Thermophoresis, are investigated and compared. The numerical values for velocity, temperature, skin friction coefficient, concentration, Sherwood number, and Nusselt number are tabulated and visually represented. Our findings showed that chemical reactions, heat generation or absorption, buoyancy force thermal expansion, and buoyancy force concentration expansion all had an impact on magne-

tohydrodynamics of a nanofluid over a stretching sheet. We recommend the use of the SLLM in solving problems of MHD flows because it is fast and effective. However, other types of equations, such as time-dependent evolution equations, partial differential equations, and difference equations, require the procedure to be extended. For future studies we can try to compact finite difference schemes on SLLM to see if it can be effective and faster.

Bibliography

[1] Abdelhalim E., Mutairi F. A, and Khaled S. M.: Effect of Velocity Slip Boundary Condition on the Flow and Heat Transfer of Cu-Water and TiO2-Water Nanofluids in the Presence of a Magnetic Field, *Hindawi Publishing Corporation , 2014, 1 - 9, (2014).*

[2] Alfvén H., existence of electromagnetic hydrodynamic wawes, *Nature 150(3805), 405 - 406 (1942).*

[3] Alsaedi A., Awais M. and Hayat T: Effects of heat generation/absorption on stagnation point flow of nanofluid over a surface with convective boundary conditions, *Communications in Nonlinear Science and Numerical Simulation, 17, 4210 - 4223, (2012).*

[4] Anderson J.D: Fundamental of Aerodynamics, *4th Ed. McGraw-Hill, (2007).*

[5] Anderson Jr J. D.: Introduction to Flight, *5th ed., McGraw-Hill Higher Education, Boston, (2005).*

[6] Anuar I: MHD Boundary Layer Flow Due to an Exponentially Stretching Sheet with Radiation Effect, *Sains Malaysiana, 4, 391 – 395, (2011).*

[7] Anwar I. Qasim F. R. and Mohl Z. S.: Chemical reaction and uniform heat generation or absorption effects on MHD stagnation-point flow of a nanofluid over a porous sheet, *World Applied Science Journal 24, 10, 1390 - 1398, (2013).*

[8] Brinker C.J, George W. and Scherer W., Sol-Gel Science: The Physics and Chemistry of Sol-Gel Processing, *Elsevier's Science and Technology,* 1_{st} *ediction, New York, 1990.*

[9] Chamkhab J. A., Magyaria E.: Combined effect of heat generation or absorption and first-order chemical reaction on micropolar fluid flows over a uniformly stretched permeable surface: The full analytical solution, *International Journal of Thermal Sciences, 49, 1821 - 1828, (2010).*

[10] Choi S.U.S: Enhancing Thermal Conductivity of Fluids with Nanopartitcles, *ASME, New York, 10, 99 - 105, (1995).*

[11] Cortell R: MHD flow and mass transfer of an electrically conducting fluid of second grade in a porous medium over a stretching sheet with chemically reactive species, *Chemical Engineering and Processing: Process Intensification, 46, 721 - 728, (2007).*

[12] Das S., Jana R.N. and Makinda O.D: MHD boundary layer slip flow and heat transfer of nanofluid past a vertical stretching sheet with non-uniform heat generation/absorption, *International Journal of Nanoscience, 13, https://doi.org/10.1142/S0219581X14500197, 2014.*

[13] Dharmendar R., Rao V. S. and Babu L. B: MHD boundary layer flow of nanofluid and heat transfer over a porous expontially stretching sheet in presence of thermal radiation and chemical reaction with suction, *International Journal of Mathematics Trends and Technology, 47, 645 – 647, (2017).*

[14] Derobert X, Dumoulin J: Electromagnetic Methods, Evaluation of Civil Engineering Structures, *Elsevier, 87-137, (2018).*

[15] Dodda R., Srinivasa R, Anand R. J. and Rashidi M. M.: Boundary layer viscous flow of nanofluids and heat transfer over a nonlinearly isothermal stretching sheet in the presence of heat generation/absorption and slip boundary condition, *Int. Nanosci Nanotechnol, 12, 251 - 268, (2016).*

[16] Ferdows M., Shakhaoath Khan Md., Mahmud Alam Md. and Afify A. A.: MHD boundary layer flow and heat transfer characteristics of a nanofluid over a stretching sheet, *ACTA UNIV. SAPIENTIAE, MATHEMATICA, 9, 140 - 161, (2017).*

[17] Goyal M, Gurjar G, Tailor Y : Heat and mass transfer of free convective micropolar fluid flow over a shrinking sheet, *Proceedings of International Conference on Advancements in Computing and Management (ICACM), 2019, 738 - 746, (2019).*

[18] Gnaneswara R. M, Sandeep N: Computational modelling and analysis of heat and mass transfer in MHD flow past the upper part of a paraboloid of revolution. *Eur. Phys. J. Plus, 132, 1 - 18, (2017).*

[19] Ibrahim W., Tulu A.: Magnetohydrodynamic (MHD) Boundary Layer Flow Past a Wedge with Heat Transfer and Viscous Effects of Nanofluid Embedded in Porous Media, *Hindawi, 1 - 12, 2019.*

[20] Islam M., Rafiqul: State-of-the-art of drilling, *Advances in Mathematical Physics, 2020, 1 - 16, (2021).*

[21] Ibrahim W, Negera M: The Investigation of MHD Williamson Nanofluid over Stretching Cylinder with the Effect of Activation Energy, The full analytical solution, *Advances in Mathematical Physics, 2020, 1 - 16, (2020).*

[22] Jiyuan Tu, Guan-heng Y and Chaoqun L: Governing Equations for CFD: Fundamentals, *Elsevier BV, Australia, (2018).*

[23] Khaled S. M., Wang, L., Fan, J.: Heat Conduction in Nanofluids, Structure-Property Correlation, *Int. J. Heat Mass Transf., 54, 4349 - 4359, (2011).*

[24] Khanba A., Maboodaw F., Ismaila I. M.: MHD boundary layer flow and heat transfer of nanofluids over a nonlinear stretching sheet: A numerical study, *Journal of Magnetism and Magnetic Materials, 374, 569 - 576, (2015).*

[25] Khaled S. M.Kleinstreuer C., Feng Y.: Experimental and Theoretical Studies of Nanofluid Thermal Conductivity Enhancement, *Nanoscale Res Lett, 6, 229 - 241, (2011).*

[26] Kumarann G., Sandeep M.: Computational analysis of magnetohydrodynamic Casson and Maxwell flow over stretching sheet with cross diffusion, *Journal in Physics, 6, 147 - 155, (2017).*

[27] Kuppala R., Sekhar G., Viswanatha Reddy S.V.K.Varma: Effects of Heat Generation/Absorption on Heat and Mass Transfer along a Moving Vertical Surface in the Presence of Chemical Reaction, *Chemical and Process Engineering Research , 36, 26 - 30, (2015).*

[28] Kasmani R. M., Sivasankaran S., Bhuvaneswari M. and Siri Z.: Effect of Chemical Reaction on Convective Heat Transfer of Boundary Layer Flow in Nanofluid over a Wedge with Heat Generation/Absorption and Suction, *Journal of Applied Fluid Mechanics, 9, 379 - 388, (2016).*

[29] Landau L.D, Litshitz E.M :Fluid mechanics, *course of theoredical physics (2nd ed),6, 551, New York, (1987).*

[30] Hari R., Katariaa H., Patel R.: Effects of chemical reaction and heat generation/absorption on magnetohydrodynamic (MHD) Casson fluid flow over an exponentially accelerated vertical plate embedded in porous medium with ramped wall temperature and ramped surface concentration, *Propulsion and Power Research, 8, 35 - 46, (2018).*

[31] Mdziniso M., "The new Spectral Adomain decomposition method and its higher order based iterative schemes for solving highly nonlinear two-point boundary value problems", *University of Johannesburg, (2013).*

[32] Mohammed R. E. D.: Chemical reaction effect on MHD boundary layer flow of two-phase nanofluid model over an exponetially stretchung sheet with a heat generation, *Journal of Molecular Liquids, 220, 718 - 725, (2016).*

[33] Mohanty J., Das J. K., Mishra S. R: Chemical reaction effect on MHD jeffery fluid over a stretching sheer with heat generation/absorption, *AMSE JOURNALS, 83, 1 - 17, (2014).*

[34] Muriuki C: MHD flow and heat transfer of a Newtonian fluid passing through parellel porous is plate in presence of an inclined magnetic field, *Australian Journal of Basic and Applied Sciences, 39, 121 - 128, (2014).*

[35] Motsa S: A New Spectral Relaxation Method for Similarity Variable Nonlinear Boundary Layer Flow Systems, *Journal Chemical Engineering Communications, 201, 241 - 256 (2014).*

[36] Motsa S., Shateyi S., Makukula Z.: On spectral relaxation method for entropy generation on a MHD flow and Heat transfer of a Maxwell fluid, *Journal of Applied Fluid Mechanical, 8, 22 - 31, (2015).*

[37] Parimal P.: Industrial Water Treatment Process Technolgy, Butterworth-Heinemann, *Elsvier, 145 - 171, (2017).*

[38] Ravindran R., Ganapathirao M., Pop I.: Effect of chemical reaction and heat generation/absorption on unsteady mixed convection MHD flow over a vertical cone with non-uniform slot mass transfer, *International Journal of Heat and Mass Transfer, 73, 743 - 751 (2014).*

[39] Sarojamma G. Mahaboobjan, S., Nagendramma V.: Influence of hall currents on cross diffusive convection in a MHD boundary layer flow on stretching sheet in porous medium with heat generation, *International Journal of Mathematics Archive, 3, 227 - 248 ,(2015).*

[40] Shagaiya D. Y.: Steady MHD boundary-layer slip flow and heat transfer of nanofluid over a convectively heatedof a non linear permeable sheet, *Journal of Advanced Mechanical Engineering, 39, 791 - 799, (2016).*

[41] Shateyi S, Mukwevho N: Numerical analysis of unsteady MHD mixed convection flow past an infinite vertical plate in the presence of dufour and soret efferts with viscous dissipation, *JP Journal of Heat and Mass Transfer, 1, 19 - 41, (2019).*

[42] Shateyi S., Marewo G. T.: Unsteady MHD flow near a stagnation point of two dimensional porous body with heat and mass transfer thermal radiation and chemical reaction, *Boundary Value Problem Hindawi, 1, 2 - 18, (2014).*

[43] Shateyi S., Mabood F., Rashidi M. M., Momoniat E., Freidoonimehr N.: MHD stagnation point flow heat and mass transfer of nanofluids in porous medium with radiation, viscous dissipation and chemical reaction, *Advanced Powder Technology, 27, 742 - 749, (2011).*

[44] Shateyi S.: MHD flow of a Maxwell fluid past a vertical stretching sheet in the presence of thermophoresis and chemical reaction, *Boundary Value Problems, https://doi.org/10.1186/1687-2770-2013-196, 196, 2 - 14 (2013).*

[45] Shateyi S., Motsa S., Sibanda P.: Homotopy Analysis of Heat and Mass Transfer Boundary Layer Flow Through a Non-Porous Channel With Chemical Reaction and Heat Generation, *Can. J. Chem. Eng., 6, 975 – 982, (2010).*

[46] Shateyi S, Motsa S.: Unsteady magnetohydrodynamics convective heat and mass transfer past an infinite vertical plate in a porous medium with thermal radiation heat generation/absorption and chemical reaction, *Advanced topic in mass transfer intech open. 145 - 162, 2011*

[47] Shateyi S., Motsa S.: Advanced Topics in Mass Transfer, Unsteady MHD convective heat and mass transfer past an infinite vertical plate in a porous medium with thermal radiation, heat generation and chemical reaction, *IntechOpen, 146 - 162, (2011).*

[48] Sudipta G, Swati M: MHD mixed convection flow of a nanofluid past a stretching surface of variable thickness and vanishing nanoparticle flux. *Pramana – J. Phys, 91, 61, (2020).*

[49] Sudarsana P. R, Chamkha A. J, Al-Mudhaf A: MHD heat and mass transfer flow of a nanofluid over an inclined vertical porous plate with radiation and heat generation/absorption. *Advanced Powder Technology, 28, 1008 - 1018, (2017).*

[50] Trefethen L. N.: Spectral methods in MATLAB, *SIAM , Philadelphia, (2000).*

[51] Vaidya H , Rajashekhar C, Manjunatha G, Prasad K.V, Makinde O.D , Vajravelu K: Heat and mass transfer analysis of MHD peristaltic flow through a complaint porous channel with variable thermal conductivity, *Phys. Scr., 95, 1 - 11, (2020).*

[52] William S., Anna J., Melisa M., Simpson M.: Newtonian and non-Newtonian fluids: velocity profiles, viscosity data, and Laminar flow friction factor equations for flow in a circular duct. *ASME: International Mechanical Engineering, University of Memphis Memphis, Tennessee USA, 2008.*

[53] Wongwise S. A. and Daungthongsuk W: Critical review of convective heat transfers nanofluids, *Renewable and Sustainable Energy Reviews, Elsevier, 11, 797 - 817, (2007).*

[54] Yang L, Huang J, Mao M: Investigations of a new combined application of nanofluids in heat recovery and air purification, *Powder Technology, 360, 956 - 966, (2020).*